

Modeling the emergence of polarity patterns in meristemic auxin transport

Silvia Grigolon ^{1,*}, Peter Sollich ^{2,†}, Olivier C. Martin ^{3,‡}

¹ *LPTMS - Laboratoire de Physique Théorique et Modèles Statistiques,*

Univ Paris - Sud, 15, Rue Georges Clémenceau, 91405 Orsay CEDEX, France,

² *Department of Mathematics, King's College London, Strand, London, WC2R 2LS UK,*

³ *INRA, UMR 0320/UMR 8120, Génétique Végétale,*

*Univ Paris - Sud, F-91190 Gif - sur - Yvette, France**

Morphogenesis in plants is initiated in meristems, the cells there differentiating under the influence of signals from the hormone auxin. Auxin is actively transported throughout the meristem via dedicated transporters such as PIN. In the last decade it has been discovered that this transport is highly polarised, nearby cells driving auxin flux in similar directions. Here we provide a model of both the auxin transport and of the dynamics of cellular polarisation based on flux sensing. Our main findings are: (i) spontaneous PIN polarisation arises if and only if cooperative effects in PIN recycling are strong enough, (ii) there is no need for an auxin concentration gradient, and (iii) orderly multi-cellular patterns of PIN polarisation are favored by molecular noise.

arXiv:1411.0733v1 [q-bio.TO] 3 Nov 2014

* silvia.grigolon@lptms.u-psud.fr; † peter.sollich@kcl.ac.uk; ‡ olivier.martin@moulon.inra.fr

CONTENTS

I. Introduction	2
II. The model of auxin dynamics and PIN recycling	3
III. Analysis of the one-dimensional model	7
A. Dynamical equations	7
B. Steady-state auxin concentrations given translation-invariant PIN configurations	7
C. Translation-invariant dynamics of PIN in the quasi-equilibrium limit for auxin	8
D. Spontaneous symmetry breaking and phase diagram for translation-invariant steady states	9
E. Non translation-invariant steady states	11
F. Properties of the stochastic model	12
IV. Analysis of the two-dimensional model	13
A. Steady-state auxin concentrations given translation-invariant PIN configurations	13
B. Translation-invariant dynamics of PIN in the quasi-equilibrium limit for auxin	14
C. Spontaneous symmetry breaking and phase diagram for translation-invariant steady states	15
D. Non translation-invariant steady states	16
E. Properties of the stochastic model	17
V. Conclusions	18
VI. Acknowledgements	19
References	19
Supplementary Material to: Modeling the emergence of polarity patterns in meristemic auxin transport	20
A. Linearized auxin dynamics for given PIN configurations	20
1. Dynamical equations	20
2. Cell-cell couplings are ferromagnetic	23
B. Critical line in the phase diagram	24
C. Polarisation Angle Susceptibility in the two-dimensional Model	25

I. INTRODUCTION

In plants, the initiation of different organs such as roots, leaves or flowers arises in regions called meristems [1–3]. These regions contain stem cells that have the potential to proliferate and differentiate into any of the plant’s organs throughout the whole life of the plant. The choice of which organ is initiated depends on the cues received by the cells, be they from the environment or as signals produced by the plant itself [4]. Amongst these signals, the hormone auxin plays a central role. Auxin was discovered over a half century ago along with some of its macroscopic effects on leaf and root growth [5]. Its local accumulation leads to cell differentiation and commitment to the initiation of new organs [6, 7]. Like a number of other molecular species, auxin is actively transported inside meristems and the resulting distribution of this hormone is ultimately key to the plant’s architecture.

In the past decade, much has been learned about the molecular actors controlling auxin movement in meristems. First, cell-to-cell auxin fluxes depend on two classes of transporters [8–10]: (i) PIN, that pumps auxin from inside to outside cells [11], and (ii) AUX1, that pumps auxin from outside to inside cells. Second, auxin accumulation drives cell proliferation and differentiation; observations have shown that auxin accumulates according to near deterministic patterns. Third, cells are polarized for their PIN content, that is PIN transporters localize mainly to one side of cells [1]. In addition, these polarizations are similar from cell to cell so that auxin is systematically transported along the direction of this polarization. That *ordering* has major consequences for the morphogenesis induced within the meristem because it affects the distribution of auxin, and auxin drives the initiation of promordia which themselves produce the new organs [12, 13]. Much work has focused on how PIN polarization patterns lead to auxin distributions, but two major questions remain unanswered concerning the emergence of PIN polarization patterns: (i) Can PIN

become polarized in cells in the absence of auxin gradients? (ii) Can PIN polarization patterns be coherent on the scale of many cells?

To address these questions, we take a modeling approach here, incorporating the main ingredients of what is currently known about (i) intercellular auxin transport and (ii) intracellular PIN dynamics. We will first provide a deterministic framework using differential equations for modeling the dynamics of auxin and of PIN cellular polarization. Our model exhibits multiple steady states which we characterize, the simplest ones being translation-invariant with all cells having the same polarization for PIN. We find that the emergence of polarization depends on the degree of cooperative effects within the PIN recycling dynamics. We then include molecular noise in this system coming from the stochastic dynamics of PIN intra-cellular localization. Interestingly, for biologically realistic values of the model's parameters, the system is driven into a state where cells coherently polarize in the same direction. In effect, the noise selects for a robust self-organised state having homogeneous PIN polarization, corresponding to a noise-induced ordering scenario.

II. THE MODEL OF AUXIN DYNAMICS AND PIN RECYCLING

Auxin transport in shoot meristems takes place mainly in a sheet that consists of a single layer of cells and which is referred to as the L1 layer [2, 3, 14–16]. We shall therefore work using a single layer of cells to represent the meristem. Our model of the Shoot Apical Meristem (SAM) starts with a lattice of cubic cells of side Λ separated by apoplasts – the space between two adjacent cells – of width λ (*cf.* Fig. 1 which represents a view from above of this system). Tissues consist of closely packed cells so $\lambda \ll \Lambda$; typical values are $\lambda \approx 1\mu\text{m}$ and $\Lambda \approx 20\mu\text{m}$. It has long been known that the hormone auxin is an important morphogen for plant development and more specifically that it is the key driver of meristemic dynamics [6]. It is subject to different processes:

- production and degradation inside cells, with rate constants β and ρ ;
- passive diffusion within cells, within apoplasts, and also between cells and apoplasts;
- active transport across cell membranes via transporters.

Since cell membranes form barriers to exchanges of molecules, taking a molecular species from one side to the other often requires dedicated transporters. In the case of auxin, the cell membrane does allow some amount of diffusion of the hormone but much less than the inside of the cell or of the apoplast where diffusion is very rapid. We call D the associated diffusion constant (measured in $\mu\text{m}^2/\text{s}$) *within* the membrane of thickness ϵ whereas formally we consider diffusion inside cells and inside apoplasts to arise infinitely quickly; as a consequence, intra-cellular variations of auxin concentration are negligible and so are those within an apoplast. In addition, auxin is subject to active processes that transport it across the cell membrane. Experimental evidence has shown that there are different molecular transporters for the in-going and out-going fluxes, transporters called respectively *AUX1* and *PIN* [7, 17]. These transporters are normally localised on the cell membrane where they can play their role to actively transport auxin between the inside and the outside of the cell. The out-going transporters belong to a large family, each member specializing to different organs and tissues of the plant [18]: in our context, we will refer to these transporters simply as PIN [19], PIN1 being the best studied member.

The dynamics for auxin concentration in each region (cell or apoplast) is then specified by the trans-membrane fluxes of auxin along with production and degradation terms. In the case of cells, we have

$$\frac{dA_c(P,t)}{dt} = \beta - \rho A_c(P,t) + \Lambda^{-1} \sum_{P'} [\phi_{AUX1}(P,P') - \phi_{PIN}(P,P') + D(A_a(P,P',t) - A_c(P,t))/\epsilon]. \quad (1)$$

In this equation, $A_c(P,t)$ is the auxin intra-cellular concentration of the cell centered at position $P = (x,y)$ at time t , and $A_a(P,P',t)$ is the auxin concentration in the apoplast separating nearest neighbor cells P and P' . Both concentrations will be specified in micro-moles per liter (μM for micro-molar). Furthermore, only the diffusion constant of auxin *within* the cell membrane appears because it is far smaller than that within a cell or apoplast. $\phi_{AUX1}(P,P')$ and $\phi_{PIN}(P,P')$ are the auxin flux *densities* carried by the transporters through a cell's "face", *i.e.*, the area of the membrane of cell P that faces cell P' . By convention, the sign of each flux is positive, the one for PIN going from the inside to the outside of the cell, and the one for AUX1 going from outside to inside the cell. These flux densities have units of μM per second per surface area (μm^2). The sum over cells P' is restricted to the neighbors of P so in effect one sums over all sides of the cell P under consideration that connect to the rest of the system. The parameters β and ρ are the rates of auxin production and degradation. In addition, the factor Λ^{-1} appears because one goes from flux densities across a cell face to effects on the concentrations inside cells. Lastly, in our framework as depicted in Fig. 1, apoplasts connect only to cells and vice versa, there are no cell-to-cell contacts nor apoplast-to-apoplast contacts.

In a similar fashion, the concentration $A_a(P, P', t)$ of auxin in the apoplast separating cells P and P' obeys the differential equation:

$$\frac{dA_a(P, P', t)}{dt} = \lambda^{-1}[\phi_{PIN}(P, P', t) - \phi_{AUX1}(P, P', t) + \phi_{PIN}(P', P, t) - \phi_{AUX1}(P', P, t) + D(A_c(P, t) + A_c(P', t) - 2A_a(P, P', t))/\epsilon]. \quad (2)$$

Note that there is neither production nor degradation of auxin in the apoplast (it is a passive medium and auxin has a long lifetime in the absence of the active degradation processes present in cells).

In *Arabidopsis*, which currently is the most studied plant, flux due to the AUX1 influx transporter seems to be several times higher than that due to passive diffusion [20, 21], thus active processes are probably the main drivers of auxin distribution. Furthermore, the transporters AUX1 and PIN are believed to be completely unidirectional; the associated molecular mechanisms are unclear but involve first the binding of auxin and then conformational changes. Because these processes are analogous to enzymatic reactions, we model the associated auxin fluxes via irreversible Michaelis-Menten kinetics:

$$\Lambda^2 \phi_{AUX1}(P, P', t) = N^{AUX1} \cdot \alpha \cdot \frac{A_a(P, P', t)}{1 + \frac{A_a(P, P', t)}{A^*} + \frac{A_c(P, t)}{A^{**}}}, \quad (3)$$

$$\Lambda^2 \phi_{PIN}(P, P', t) = N^{PIN} \cdot \gamma \cdot \frac{A_c(P, t)}{1 + \frac{A_a(P, P', t)}{A^*} + \frac{A_c(P, t)}{A^{**}}}, \quad (4)$$

where α and γ are kinetic constants analogous to catalysis rates. The factor Λ^2 on the left-hand side of these equations is the surface of the face of each cell, and connects the flux *density* to the (absolute) flux. At a molecular level, N^{AUX1} (respectively N^{PIN}) refers to the *number* of AUX1 (respectively PIN) transporters on the area of P 's membrane which faces cell P' . Finally, A^* and A^{**} play the role of Michaelis-Menten constants associated with saturation effects; these could have been taken to be different in Eqs. 3 and 4 without any qualitative consequences for the model's behavior.

We are not aware of any experimental evidence that the distribution of AUX1 transporters changes with time or that these transporters contribute to cell polarity. Thus we shall assume that their numbers are constant on each face of the cell. In contrast, PIN transporters are particularly important for driving morphogenesis through the formation of polarity patterns. Often they define clear polarized fields in tissues [14, 22] where cells see their PINs predominantly localised to one of their faces, the face being the same for many cells. That polarity leads to coherent auxin transport, accumulation of auxin in specific regions, and then the first signs of commitment to differentiation in the form of primordia [23, 24]. To take into account this possibility of forming polarized distributions of PIN, we introduce the four faces of a cell as R for right, U for upper, L for left and D for down. (The two faces parallel to the L1 layer play no role in our simplified modeling.) Then each face of a cell has a potentially variable number of PIN transporters:

$$N_f^{PIN}, \quad f = R, U, L, D.$$

Furthermore we impose the constraint $\sum_f N_f^{PIN} \equiv \sigma$, a cell-independent constant so each cell has the same number of PIN transporters at all times.

The dynamics of PIN seem complex: it is known that PINs are subject to ‘‘recycling’’ within a cell through different mechanisms including transport from the membrane to the golgi apparatus and back to the membrane [10, 25–27]. Most modeling takes PIN dynamics to be driven by surrounding auxin concentrations [15, 16, 20, 21, 28, 29]. For instance it has been postulated that PIN might accumulate to the membrane facing the neighboring cell with the highest concentration of auxin [15, 16]. As a consequence, the presence of an auxin gradient becomes a necessary condition for PIN polarization. Here we consider instead dynamics based on *flux sensing* where PIN recycling rates are modulated by the amount of auxin flux transported by those same PIN transporters. Mathematically, we take the PIN dynamics on a face f ($f = R, U, L, D$) of a cell to be specified as follows:

$$\tau \frac{dN_f^{PIN}}{dt} = -\frac{3}{4} N_f^{PIN} \frac{1}{1 + \left(\frac{\phi_f^{PIN}}{\phi^* \Lambda^{-2}}\right)^h} + \frac{1}{4} \sum_{f'} N_{f'}^{PIN} \frac{1}{1 + \left(\frac{\phi_{f'}^{PIN}}{\phi^* \Lambda^{-2}}\right)^h}. \quad (5)$$

These differential equations model the competitive recycling of the PINs amongst the faces of a given cell in a flux dependent manner. Note that τ is the characteristic time scale of the recycling process and that the dynamics enforce the constraint of conservation of the total number of PIN transporters inside each cell. Also, in Eq. 5, ϕ_f^{PIN} is the flux $\Lambda^2 \phi_{PIN}$ (not a flux density) flowing through face f while ϕ^* is a constant.

β	$1 \mu\text{M} \cdot \text{day}^{-1}$
ρ	1 day^{-1}
α	$0.1 \text{ L} \cdot \text{s}^{-1}$
γ	$10^{-4} \text{ L} \cdot \text{s}^{-1}$
A^*	$2 \times 10^{-3} \mu\text{M}$
A^{**}	$0.8 \mu\text{M}$
ϕ^*	$1.6 \times 10^{-5} \mu\text{mole} \cdot \text{s}^{-1}$
N^{AUX1}	200
σ	1000
Λ	$20 \mu\text{m}$
λ	$1 \mu\text{m}$
ϵ	10 nm
τ	30 min

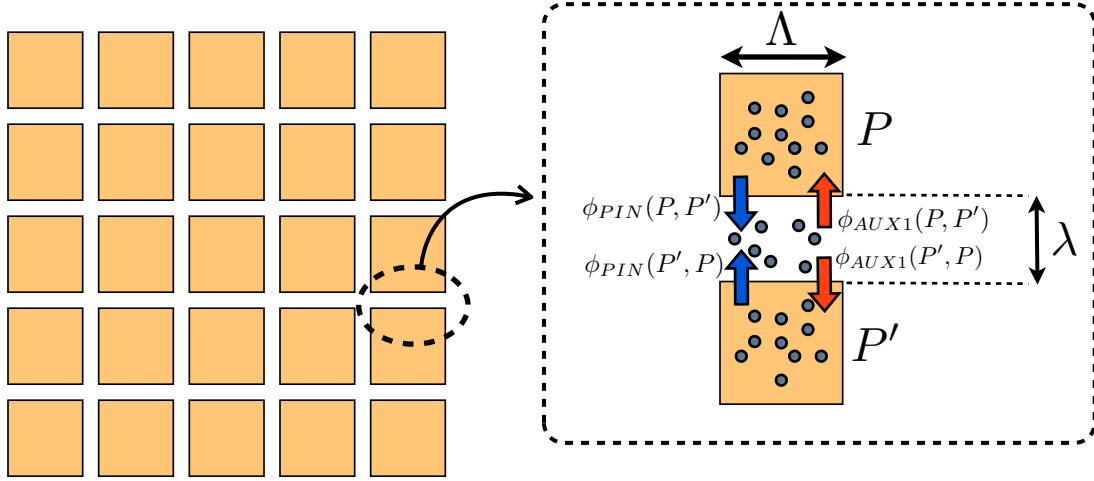
TABLE I: Parameters used in the model. M stands for *molarity*, *i.e.*, number of moles per liter. L stands for liter.

To understand the consequences of Eq. 5, consider first the low flux limit, ϕ_f^{PIN} being small for all faces, so that all denominators can be ignored. At a molecular level, each transporter leaves the cell membrane at a rate proportional to τ^{-1} ; transporters are then brought into the cytoplasm or golgi apparatus; finally they get reallocated randomly to any of the 4 faces. In such a low flux regime, cells will show no PIN polarization. Second, consider instead the case where for at least one face f , $\phi_f^{PIN}/\phi^*\Lambda^{-2}$ is large. That face will *benefit* from the recycling, recruiting more transporters from the other faces than it loses. ($\phi^*\Lambda^{-2}$ is just the scale at which flux sensing in this system becomes important). At an individual transporter level, the competitive recycling means that transporters which are actively shuttling auxin see their rate of recycling go down. How this happens depends on unknown molecular details, nevertheless, the rate of detachment of a transporter from the membrane probably depends on what fraction of the time it is binding auxin and thus the rate of detachment will show a dependence on ϕ^{PIN} . One may attempt to model this via a simple hyperbolic law to describe saturation effects. To be still more general, we have further introduced a Hill exponent, h . Such a functional form is often used for modeling binding rates and then h is an integer related to the number of molecules that must co-localize, but more generally h can be used to simply parametrize cooperative effects. In the absence of detailed knowledge of the molecular mechanisms controlling PIN recycling, we use this phenomenological form and will see whether or not h plays an important role.

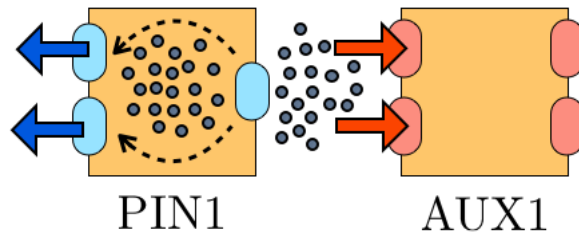
The model is now completely specified and involves the 15 parameters Λ , λ , ϵ , α , β , γ , ρ , A^* , A^{**} , ϕ^* , τ , σ , N^{AUX1} , D , and h . Some of these parameters can be absorbed in scale changes. Nevertheless, to keep the physical interpretation as transparent as possible, we stay with the dimensional form of the equations. Whenever possible, we assign values to the parameters using published estimates or compilations thereof [30]. For instance, mass-spectrometry measurements [31] in very young leaves quantify the concentration of auxin to be about 250 picograms per milligram of tissue. Since the molecular mass of auxin is about 175, A_c is of the order of 1 micro-molar. As we shall see, in the steady-state regime, $\beta/\rho = A_c$, a relation providing a constraint on those two parameters. Furthermore, a direct estimate of β follows from isotopic labeling measurements [31] which show that biosynthesis replenishes auxin within about one day; we have thus set $\beta=1/\text{day}$. Unfortunately, for many parameters no such experimental data is available. For most such cases, we use ball-park estimations that seem reasonable. However, for h , which provides a phenomenological parameterization of cooperative effects in PIN recycling, we have little choice but to study the behavior of the model as a function of its value. We use the same strategy for D . Thus, both D and h will be used as control parameters, allowing us to map out a two-dimensional phase diagram. For instance, when increasing D , passive diffusion will overcome the effects of active transport, allowing one to probe the importance of active *vs.* passive transport in the establishment of PIN polarization. Unless specified otherwise, all other parameter values are set as provided in Table I.

Since our aim is to understand how organised polarity patterns arise in a system described by this model, it is appropriate to define something like an order parameter to quantify the ordering of flux directions or PIN intracellular localisation. We thus introduce the two-dimensional *polarization* vector $\vec{\delta}$ for a cell at position $P = (x, y)$; its components depend on the face-to-face difference of the number of PINs along each direction (say horizontal or vertical) in the following way:

$$\vec{\delta}(x, y) \equiv \begin{cases} \delta_1(P) = \frac{N_R^{PIN}(P) - N_L^{PIN}(P)}{\sigma} \\ \delta_2(P) = \frac{N_U^{PIN}(P) - N_D^{PIN}(P)}{\sigma} \end{cases} \quad (6)$$



(a) Schematic representation of the model's ingredients.



(b) Role of transporters and PIN recycling.

FIG. 1: 1a Schematic two-dimensional view of the system consisting of a single layer of cells. Cubic cells of size Λ are in orange, apoplasts of width λ are in white. On the right: a zoom on two neighboring cells. Gray circles stand for auxin and red arrows represent the incoming AUX1 mediated fluxes in cells, while light blue arrows represent the outgoing PIN mediated fluxes. In these views from above, the thickness (Λ) of the cells is not shown. 1b Role of transmembrane transporters. PINs pump auxin from the inside of the cell to an adjacent apoplast. AUX1 plays the reverse role, pumping auxin from apoplasts to the inside of the cell. Dashed arrows within a cell illustrate PIN recycling.

The vector in Eq. 6 has a magnitude $|\vec{\delta}(P)| \in [0, 1]$: the two extremal values represent respectively the unpolarized case, *i.e.*, $N_f^{PIN} = \sigma/4$ for all f , and the fully polarized case, *i.e.*, $N_f^{PIN} = \sigma$ for one face while $N_f^{PIN} = 0$ for all other faces. Individual components can vary in $[-1, 1]$ and the extremal points give the maximum polarization in one direction or the other.

A first step will consist in understanding the behavior of this system in a one-dimensional framework.

III. ANALYSIS OF THE ONE-DIMENSIONAL MODEL

A. Dynamical equations

Let us replace the L1 layer, represented in Fig. 1 via a square lattice, by a *row* of cubic cells forming a one-dimensional lattice. As before, between two adjacent cells there is exactly one apoplast. Starting with Eq. 1, we see that the up and down terms no longer arise if we force all diffusion and transport to arise between cells and apoplasts. Defining Δ as the distance between two nearest-neighbor cells ($\Delta = \Lambda + \lambda$), one has:

$$\begin{aligned} \frac{dA_c(x, t)}{dt} = & \beta - \rho A_c(x, t) + \frac{D}{\Lambda \epsilon} \left[A_a(x, x + \Delta, t) + A_a(x - \Delta, x, t) - 2A_c(x, t) \right] + \\ & + \frac{1}{\Lambda} \left[\phi_{AUX1}(x, x + \Delta, t) + \phi_{AUX1}(x, x - \Delta, t) - \phi_{PIN}(x, x + \Delta, t) - \phi_{PIN}(x, x - \Delta, t) \right], \end{aligned} \quad (7)$$

where the positions P and P' of Eq. 1 have been replaced by x and $x' = x \pm \Delta$. Similarly, for apoplasts one has

$$\begin{aligned} \frac{dA_a(x, x + \Delta, t)}{dt} = & \frac{D}{\lambda \epsilon} \left[A_c(x, t) + A_c(x + \Delta, t) - 2A_a(x, x + \Delta, t) \right] \\ & - \frac{1}{\lambda} \left[\phi_{AUX1}(x, x + \Delta, x, t) + \phi_{AUX1}(x + \Delta, x, t) - \phi_{PIN}(x, x + \Delta, t) - \phi_{PIN}(x + \Delta, x, t) \right]. \end{aligned} \quad (8)$$

In this one-dimensional model, PIN is defined only on the left and right face of each cell. Given the constraint of conservation of total PIN transporters in each cell (only two faces contribute), the dynamics of PIN numbers are completely determined via the dynamics of N_R^{PIN} and there is just one independent equation for each cell:

$$\tau \frac{dN_R^{PIN}}{dt} = -N_R^{PIN} \frac{1}{1 + \left(\frac{\phi_R^{PIN}}{\phi^* \Lambda^{-2}}\right)^h} + N_L^{PIN} \frac{1}{1 + \left(\frac{\phi_L^{PIN}}{\phi^* \Lambda^{-2}}\right)^h}. \quad (9)$$

In this equation, $N_L^{PIN} = \sigma - N_R^{PIN}$ and a factor 2 arising from using Eq. 1 has been absorbed into τ . Furthermore, polarization is no longer a vector but a scalar, given by the first component of Eq. 6. It varies in $[-1, 1]$: when $\delta(x) \approx -1$, almost all the PINs are on the left-hand side of the cell, while when $\delta(x) \approx 1$ they are almost all on the right-hand side.

B. Steady-state auxin concentrations given translation-invariant PIN configurations

Assuming periodic boundary conditions, the row of cells becomes a ring; this idealization is convenient for the mathematical and phase diagram analysis. Consider the steady-state solutions of the differential equations. With periodic boundary conditions, one expects some steady states to be translationally invariant. In that situation, all quantities are identical from cell to cell and from apoplast to apoplast. We can then drop all spatial dependence in the variables, e.g., $A_c(x, t) = A_c$ for all x and t .

We consider here an arbitrary translation-invariant configuration of PIN transporters (steady-state or not). One has the following equations for steady-state auxin concentrations:

$$\begin{cases} 0 = \beta - \rho A_c + \frac{2D}{\Lambda \epsilon} (A_a - A_c) + \frac{2\alpha}{\Lambda^3} N^{AUX1} \frac{A_a}{1 + \frac{A_a}{A^*} + \frac{A_c}{A^{**}}} - \frac{\gamma}{\Lambda^3} \sigma \frac{A_c}{1 + \frac{A_a}{A^*} + \frac{A_c}{A^{**}}} \\ 0 = \frac{2D}{\lambda \epsilon} (A_c - A_a) - \frac{2\alpha}{\lambda \Lambda^2} N^{AUX1} \frac{A_a}{1 + \frac{A_a}{A^*} + \frac{A_c}{A^{**}}} + \frac{\gamma}{\lambda \Lambda^2} \sigma \frac{A_c}{1 + \frac{A_a}{A^*} + \frac{A_c}{A^{**}}} \end{cases}. \quad (10)$$

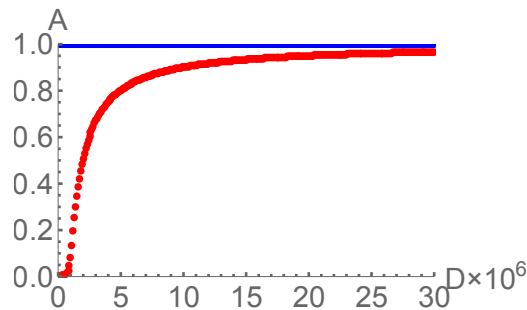


FIG. 2: Auxin steady-state concentrations (red for apoplasts and blue for cells) in an arbitrary PIN translation-invariant configuration as a function of the diffusion constant D in $\mu\text{m}^2/\text{s}$. The other relevant model parameters are given in Table I.

Note that because we imposed translation invariance, the equations do not depend on the particular values of N_f^{PIN} because all that matters here is the total number of PIN transporters per cell. These two equations determine A_c and A_a . Since in apoplasts there is no source or degradation of auxin, in the steady state the total flux (transport and diffusion counted algebraically) through an apoplast vanishes and the same holds for cells. Thus within cells auxin degradation must compensate exactly auxin production, leading to $\beta - \rho A_c = 0$. This result, namely $A_c = \beta/\rho$, is independent of all other parameters and in particular of the PIN polarization and of D as illustrated in Fig. 2. Furthermore, since A_c is now known, the second equation can be solved for A_a .

Experimental evidence [20, 21] suggests that active transport dominates passive (diffusive) transport in *Arabidopsis*. Thus the biologically relevant regime probably corresponds to D small. In the low diffusion limit ($D \rightarrow 0$), the last equation shows that A_a goes to a limiting value that is strictly positive. (A zoom of Fig. 2 would also show this is the case.) Solving this equation using the values of the parameters in Table I, one finds that the concentration of auxin in cells is much greater than that in apoplasts because $2N^{AUX1}\alpha \gg \sigma\gamma$, *i.e.*, auxin molecules are more easily transported by AUX1 than by PIN (*cf.* the left limit in Fig. 2). One may also consider what happens when diffusion is important; clearly as $D \rightarrow \infty$, the transporters become irrelevant and the equations immediately show that A_c and A_a become equal. The overall behavior is displayed in Fig. 2.

C. Translation-invariant dynamics of PIN in the quasi-equilibrium limit for auxin

Microscopic molecular events associated with auxin transport (be they active or passive) arise on very short time scales whereas the PIN recycling requires major cellular machinery and so arises on much longer time scales. Let us therefore take the *quasi-equilibrium* limit where auxin concentrations are fast variables and thus can be assumed to take on their steady-state values given the PIN configuration. Furthermore, we take the numbers of PIN transporters to be translation invariant, so we can use the results for auxin concentrations A_c and A_a of the previous section. These being PIN independent, the auxin concentrations in fact just stay at their exact steady-state values. Consider now the dynamical equation for δ , the PIN polarization. This equation can be derived easily from the equation for N_R^{PIN} and using the constraint on PIN number conservation. Since it involves a single variable, it can always be written as a gradient descent relaxational dynamics, *i.e.*, there exists a function $\mathcal{F}(\delta)$ such that:

$$\tau \frac{d\delta}{dt} = -\frac{d\mathcal{F}(\delta)}{d\delta}. \quad (11)$$

$\mathcal{F}(\delta)$ plays the role of an effective potential. $\mathcal{F}(\delta)$ is minus the anti-derivative of the right hand side; this antiderivative can be obtained in closed form, namely

$$\mathcal{F}(\delta) = \frac{(1+\delta)^2}{4} \cdot {}_2F_1\left[1, \frac{2}{h}, 1 + \frac{2}{h}, -\left(\frac{c(1+\delta)}{2}\right)^h\right] + \frac{(1-\delta)^2}{4} \cdot {}_2F_1\left[1, \frac{2}{h}, 1 + \frac{2}{h}, -\left(\frac{c(1-\delta)}{2}\right)^h\right], \quad (12)$$

where ${}_2F_1[a, b, d, z] = \sum_{k=0}^{\infty} \frac{(a)_k (b)_k}{(d)_k k!} z^k$, $(a)_k$ is the Pochhammer symbol and $c = \frac{\gamma\sigma}{\phi^*} \frac{A_c}{1 + \frac{A_a}{A^*} + \frac{A_c}{A^{**}}}$. One can check that c scales with the inverse of the diffusion constant.

The extrema of \mathcal{F} correspond to steady states for the PIN dynamics, *i.e.*, $d\delta/dt = 0$. Maxima are unstable and minima are stable. Thus it is of interest to map out the form of \mathcal{F} as a function of the parameter values. Take for

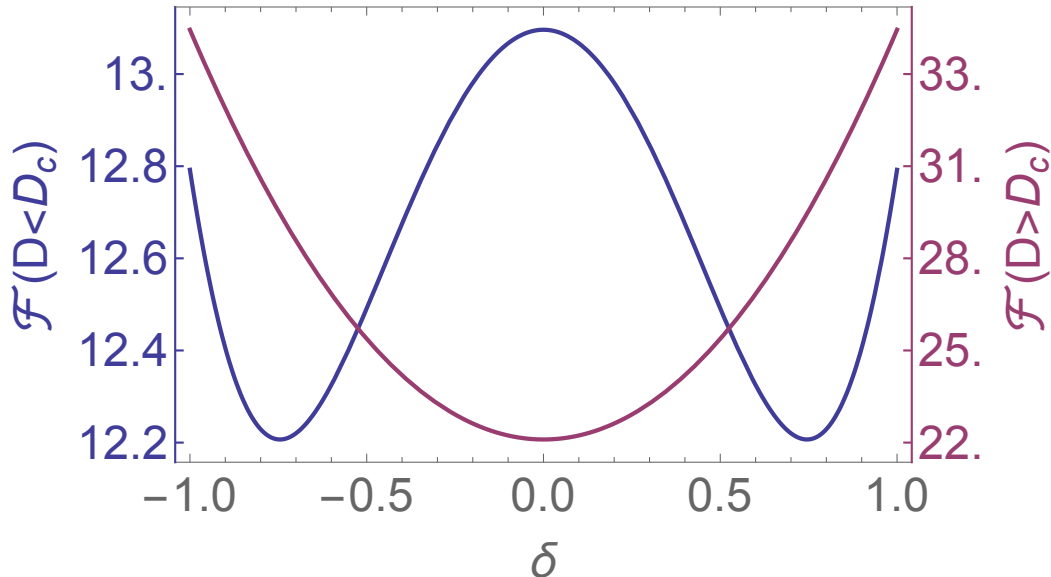


FIG. 3: Effective potential as a function of the polarization δ for $D > D_c$ (purple) and $D < D_c$ (blue). $h = 2$, other parameter values are given in Table I.

instance $h = 2$. Starting with a large value for D , use of Mathematica shows that \mathcal{F} has a single global minimum, corresponding to the unpolarized steady state, $\delta = 0$. Then as D is lowered, \mathcal{F} takes on a double-well shape, symmetric about the zero polarization abscissa where the curvature is now negative. At the same time, two new local minima appear at $\pm\delta$. Thus as D is lowered, the unpolarized state becomes unstable while two new stable steady states of polarization $\pm\delta$ appear; this situation is illustrated in Fig. 3. If we had used instead $h = 0.5$, we would have found no regime in D where \mathcal{F} has the double-well structure: there, the only steady state is the unpolarized one.

Within this framework, it is possible to determine a critical point D_c , *i.e.*, a threshold value of the diffusion constant, below which spontaneous symmetry breaking sets in. The value of D_c is obtained from the following condition (see also Supplementary Materials):

$$\frac{\partial^2 \mathcal{F}}{\partial \delta^2} \Big|_{\delta=0} = 0. \quad (13)$$

In particular, for $h = 2$, this leads to a critical value $D_c \approx 9.4 \times 10^{-7} \mu\text{m}^2/\text{s}$. This overall framework provides a convenient intuitive picture for PIN dynamics. Unfortunately no such effective potential can be obtained in the two-dimensional model as will be discussed later.

D. Spontaneous symmetry breaking and phase diagram for translation-invariant steady states

The previous formalism is complicated because of the form of \mathcal{F} . However if one is only interested in the steady states and one does not care about relaxational dynamics, the steady-state equation to solve is relatively simple (*c.f.* Eq. 9 where the left-hand side must be set to 0) and there is no need to appeal to a quasi-equilibrium approximation. We assume as before that N_R^{PIN} is translation invariant but also that it is subject to PIN recycling. Since A_c and A_a in steady states have been previously calculated, all quantities in Eq. 9 are known except for N_R^{PIN} ; it is enough then to solve the associated non-linear equation (we have used Mathematica for that). At given h not too small, we find a transition from polarized to unpolarized states as D crosses the threshold D_c (see Fig. 4 which illustrates the case $h = 2$). The position of the threshold depends on h . However, if h is too small, the transition point disappears, there are no longer any polarized steady states. To illustrate the situation, consider fixing D to a small value, say $D = 10^{-7} \mu\text{m}^2/\text{s}$, and then solve for N_R^{PIN} as a function of the Hill exponent h . For h less than a critical threshold $h_c \approx 1.09$, there is a unique solution and it corresponds to the unpolarized state, $N_R^{PIN} = N_L^{PIN} = \sigma/2$. For $h > h_c$, two new steady states appear which are polarized. These two states are related by the left-right symmetry, so one has a spontaneous symmetry breaking transition at h_c (see Fig. 5). As $h \rightarrow \infty$, these states tend towards full polarization,

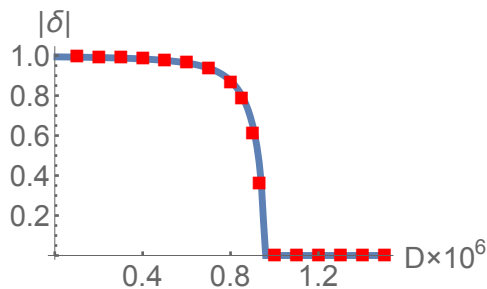


FIG. 4: Absolute value of the (translation-invariant) PIN polarization as a function of the diffusion constant D in $\mu\text{m}^2/\text{s}$ in steady states. Blue circles: analytical result using Mathematica. Red squares: result of simulating the dynamics of the model containing 20 cells on a ring until a steady state was reached; a fourth-order Runge-Kutta algorithm [32] was used, starting configurations were randomized but had positive local PIN polarizations. $h = 2$, other parameter values are given in Table I.

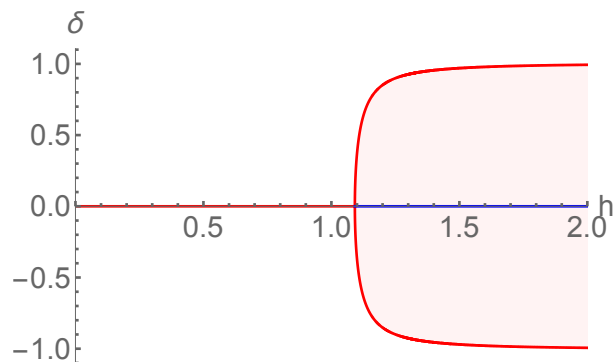


FIG. 5: Bifurcation diagram for translation-invariant states in the one-dimensional model. δ is the PIN polarization. The unpolarized state is stable for $h < h_c \approx 1.09$ (orange). Beyond that threshold, two symmetric polarized states appear. These are stable (in red) whereas the unpolarized state becomes unstable (in blue). Here $D = 10^{-7} \mu\text{m}^2/\text{s}$ while other parameter values are given in Table I.

$\delta = \pm 1$. To represent simultaneously the behavior as a function of the diffusion constant D and of the Hill exponent h , Fig. 6 provides the overall phase diagram via a heat map. Note that when h is too low *or* D is too high, the only steady state is the unpolarized one.

The origin of this spontaneous symmetry breaking is the change of stability of the unpolarized state. To quantitatively understand that phenomenon, set $N_R^{PIN} = \sigma/2 + \delta/2$ and then linearize Eq. 9 in δ . Defining $F = \gamma A_c \sigma / [2(1 + A_a/A^* + A_c/A^{**}) \frac{\phi^*}{\Lambda^2}]$ (this is a constant independent of polarization but which varies with D because of its dependence on A_a), one has $\phi_R^{PIN}/\Lambda^2 = (1 + \delta/\sigma)F$ and $\phi_L^{PIN}/\Lambda^2 = (1 - \delta/\sigma)F$. Then the linearization in δ leads to:

$$\tau \frac{d\delta}{dt} = -2 \left[\frac{1 - (h-1)F^h}{(1 + F^h)^2} \right] \delta. \quad (14)$$

Instability arises if and only if $(h-1)F^h > 1$. Note that the case of Michaelis-Menten type dynamics ($h = 1$) does *not* lead to PIN polarization. To have spontaneous polarization inside cells, one must have *cooperative* dynamics with $h > h_c = 1 + F^{-h}$ where h_c is the critical Hill exponent where the instability sets in.

One may also investigate the stability of the polarized steady state. First, within the space of translation invariant configurations, a linear stability analysis using Mathematica shows that the polarized state is always linearly stable. This is exactly what the adiabatic approximation predicts (*cf.* Fig. 3). Second, one can ask whether our translation-invariant steady states are *global* attractors when they are linearly stable. We have addressed this heuristically by simulating the dynamical equations starting from random initial conditions. When $h \leq h_c$ (or $D \geq D_c$ if one considers h as fixed), it seems that the unpolarized state is the *only* steady state and that all initial conditions converge to it. When $h > h_c$, the system seems to always go to a steady state, we have never observed any oscillatory or chaotic behavior. Sometimes these states are the previously found translation-invariant polarized states but sometimes they are not; this latter situation leads us to consider now non translation-invariant steady states.

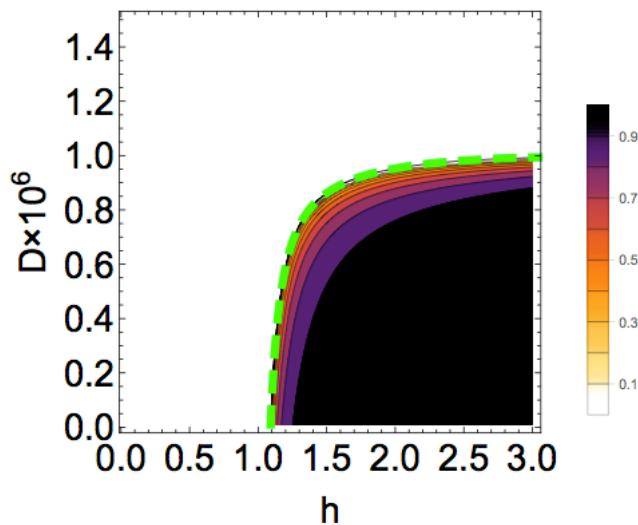


FIG. 6: Heat map of PIN polarization in translation-invariant steady states as a function of h and D in $\mu\text{m}^2/\text{s}$ rescaled by a factor 10^6 for an easier reading. Other parameter values are given in Table I. The green dashed line refers to the theoretically derived critical line.

E. Non translation-invariant steady states

If parameter values fall in the range where Fig. 6 shows high spontaneous polarization, random initial configurations will relax to steady states having quite random PIN polarizations. In effect, the coupling between neighboring cells is low in that regime and one can expect to have 2^M steady states if there are M cells. The typical steady state is then disordered, with no coherent transport of auxin. As D increases or h decreases, the number of these steady states decreases because neighboring cells more often than not have the same sign of PIN polarization. To get some insight into this phenomenon that seems analogous to ferromagnetism, let us consider what happens when a localized *defect* is introduced into an otherwise uniformly polarized system. Beginning with the uniformly polarized steady state at low D , we reverse the polarization of *one* cell to form a defect and then we let the system relax to produce the starting modified steady state. Thereafter we follow this steady state as we increase D . The resulting polarizations of the defect cell are shown in Fig. 7. We also display what happens in the absence of the defect (red curve in Fig. 7). We see that the defect cannot sustain itself arbitrarily close to the threshold D_c : when polarizations are too weak, the defect cell initially with an oppositely oriented polarization will align its polarization with its neighbors and the defect will disappear. The curve of defect polarization as a function of D_c thus has a discontinuity at some value strictly lower than D_c as can be seen in Fig. 7. The interpretation should be clear: of the 2^M putative steady states with random polarizations, some in fact do not exist, and one can expect the number of steady states to decrease steadily as one approaches D_c .

To provide further evidence in favor of such a scenario, consider what happens when there are two defects next to one another as in Fig. 8. We see that just as for the single defect, two adjacent defects disappear strictly before D_c but they do so *after* the single defect does. Another interesting feature is that the two defects have slightly different polarizations. This asymmetry is unexpected if one considers the analogy with the Ising model but in fact it is unavoidable here: indeed, the apoplast on the left of the left defect is enriched in auxin while the apoplast on the right of the right defect is depleted in auxin. We have checked that this difference vanishes if the two single-cell defects are placed far away from one another and also that in such a limit the polarization curves converge to those of single defects.

The conclusion to draw from these results is that as one approaches D_c the number of steady states diminishes. Furthermore, one expects that this effect is accompanied by a reduction in both stability and size of basin of attraction of steady states having defects, leading to an increase of the coherence length (or domain sizes where a domain is a block of cells having the same sign of polarization) as one approaches D_c . Such properties naturally lead one to ask whether noise might enhance the coherence of polarization patterns, driving the emergence of order from disorder [33].

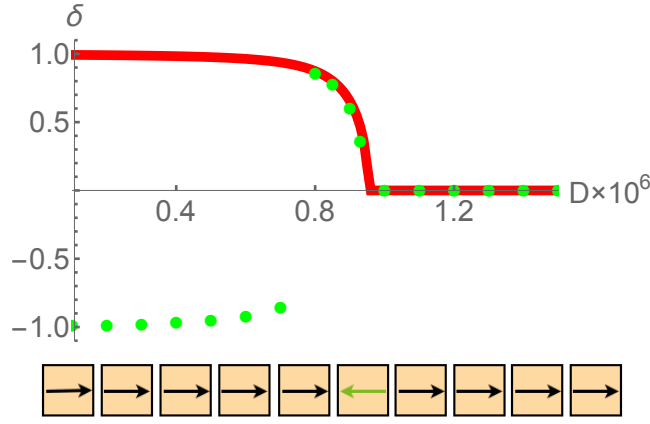


FIG. 7: PIN polarization at a defect (green) and in the absence of a defect (red) for a lattice of 20 cells as a function of D . Drawing below: initial orientation of PIN polarizations, the red arrow representing the defect. $h = 2$ while other parameter values are given in Table I.

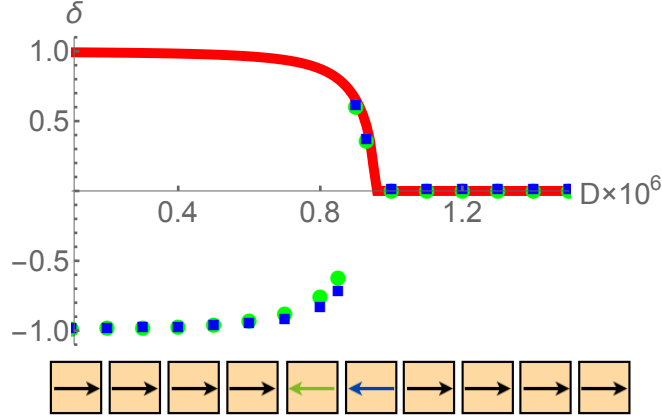


FIG. 8: PIN polarization at two adjacent defects (blue and green) and in the absence of defects (red) for a lattice of 20 cells as a function of D . Below, initial orientation of PIN polarizations, the red arrows representing the two defects. $h = 2$, other parameter values are given in Table I.

F. Properties of the stochastic model

Since the number of transporter molecules (PIN and AUX1) in our system is modest, noise in the dynamics may be important. To include molecular noise in reaction-diffusion systems, it is common practice to use a Lattice Boltzmann model framework [34] and thermodynamical considerations to render the reaction dynamics stochastic. However, in the present case, the Michaelis-Menten form of the rates of change of molecular concentrations as well as the PIN recycling dynamics do not correspond to mass action reactions so a different framework is necessary. We thus take a Gillespie-like approach [35] where each process type (production or degradation of auxin inside a cell, transfer of auxin from one side to the other of a membrane, or PIN recycling from one cell face to another) is rendered stochastic. For instance, diffusion of auxin across a face of a cell is associated with two underlying fluxes, one in each direction. If dt is a short time interval, the noiseless dynamics specifies that an average number of molecules $\mathcal{M} = rdt$ will contribute to the underlying flux where r is the rate of that process. But because of the molecular nature of the process, the true number of molecules generating that flux will be a Poisson variable of mean rdt . Applying this rule to all the underlying fluxes contributing to Eqs. 7, 8 and 9, the stochastic dynamics are naturally implemented without the introduction of any new parameters. (Note for instance that temperature dependencies feed-in only via the deterministic parameters such as D .) However, there are millions of auxin molecules in a cell and so the associated noise is negligible. In contrast, the number of PIN transporters in a cell is modest and so the noise in PIN recycling can a priori be important. Our simulation thus implements the noise in PIN recycling but not in the other processes.

The stochastic dynamics defined by the procedure just described are ergodic, so given enough time the system will

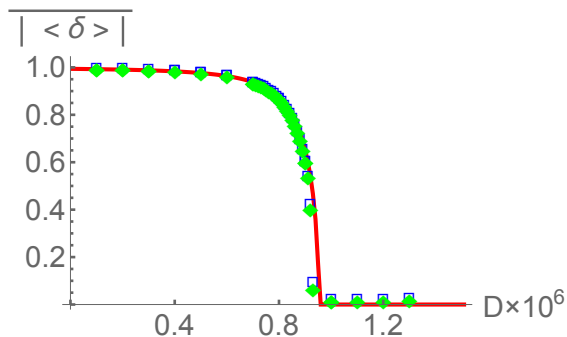


FIG. 9: Absolute value of the mean PIN polarization per site, averaged over time, as a function of diffusion for both the stochastic model for three different lattice sizes ($N_{cells} = 20$ green diamonds, $N_{cells} = 10$ blue squares) and for the deterministic model (red line). Simulations were performed using cells on a ring. $h = 2$, $\tau = 1s$, other parameter values are given in Table I.

thermalize, there being a unique “thermodynamic equilibrium state”. Although in principle this state depends on the value of τ , if auxin concentrations are close to their steady-state values which is the case here, τ just introduces a time scale and has no effect on the equilibrium state. We use simulations to study the equilibrium, putting a particular focus on the behavior of PIN polarization. Observables must be averaged over time. Just as in other thermodynamical systems having spontaneous symmetry breaking, care has to be used when extracting the order parameter. We thus measure the mean PIN polarization defined by first averaging δ over all cells to obtain $\langle\delta\rangle$, then taking the absolute value $|\langle\delta\rangle|$, and then averaging over simulation time: $|\overline{\langle\delta\rangle}|$. In practice we begin with a “cold start”, *i.e.*, the starting configuration of the system has all cells similarly polarized; then we run to thermalize the system before performing any measurements.

In Fig. 9 we show the previously defined mean polarization as a function of D for systems having 10 and 20 cells. At low D the analysis of the model in the absence of noise suggested that the system could not polarize because the typical noiseless steady state had random polarizations. Nevertheless, here we see that in the presence of noise the system seems to have a global polarization, in agreement with the order from disorder scenario [33]. If one compares to the special translation-invariant steady state in the absence of noise, it seems that noise has hardly any effect at low D , so noise can be thought of as “selecting” that particular state. As D grows, polarization intensity decreases and noise effects are amplified. As might have been expected, polarization is lost earlier in the presence of noise than in its absence. To check whether these simulations indeed are in equilibrium, we compared the polarization values to those obtained when starting the simulations with “hot starts”, *i.e.*, the starting configuration of the system having cells randomly polarized. For $D > 5 \cdot 10^{-7} \text{m}^2/\text{s}$ the two approaches agreed very well while for lower values of D the runs with random initial conditions failed to thermalize well. As a result, only for intermediate and large values of D can one be confident in the simulation.

To follow-up on this last caveat, Fig. 9 could be interpreted as suggesting that the equilibrium state in the stochastic model has a real transition between a polarized phase and an unpolarized one. However, thermalization is difficult at low D ; furthermore, for large enough numbers of cells the equilibrium state will in fact contain multiple domains of polarization, some being oriented in one direction and others in the opposite direction. This is inevitable in any one-dimensional system having short range interactions [36, 37], and so no true long range order arises in this system if the number of cells is allowed to be arbitrarily large. To add credence to this claim, note that the polarization curves are slightly different for the different lattice sizes, the polarization *decreasing* as the number of cells increases. It is thus plausible that in the limit of an infinite number of cells, the polarization vanishes for all D .

IV. ANALYSIS OF THE TWO-DIMENSIONAL MODEL

A. Steady-state auxin concentrations given translation-invariant PIN configurations

We now tackle the two-dimensional model (see Fig. 1). For each cell there are four faces contributing to active and passive transport of auxin and each allows for PIN recycling as given by Eq. 5. As for the one-dimensional model, we begin with the deterministic dynamics, again taking periodic boundary conditions for the ease of analysis. Unless otherwise specified, parameter values are set to those in Table I.

Let us first focus on auxin steady-state concentrations in the presence of translation-invariant PIN configurations.

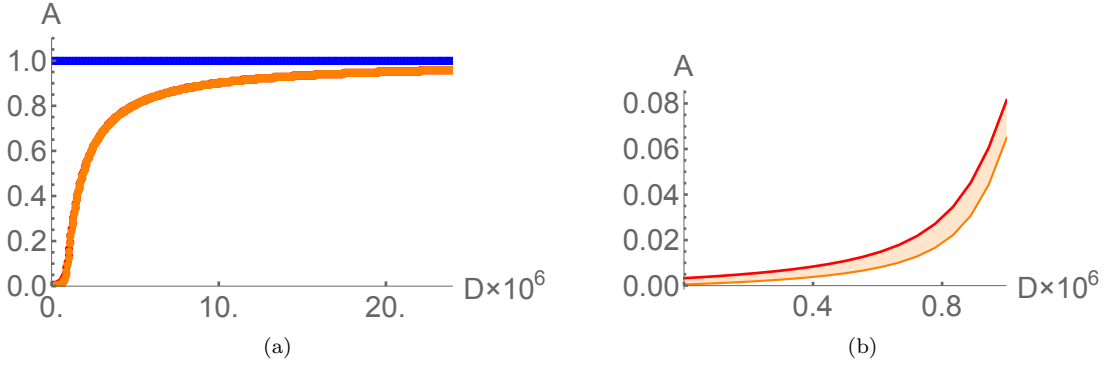


FIG. 10: Steady-state auxin concentrations in translation-invariant PIN configurations as a function of the diffusion constant D . On the left: in blue, the concentration within cells. On the left and via a zoom on the right: in red and orange, the minimum and maximum values of auxin concentration within apoplasts, arising when the number of PIN transporters facing the apoplast takes on its minimum and maximum value. $h = 2$, other parameter values as in Table I.

This allows us to drop the spatial and temporal dependence of the different variables. Thus for all (x, y) labeling cell positions of the system, one has

$$\begin{aligned} A_c(x, y) &= A_c \\ A_a^D(x, y) &= A_a^U(x, y) = A_a^U \\ A_a^L(x, y) &= A_a^R(x, y) = A_a^R \end{aligned} \quad (15)$$

where $A_a^R(x, y)$ (respectively $A_a^U(x, y)$) is the right (respectively up) apoplast auxin concentration when considering the cell at position (x, y) .

In all steady states, the total rate of auxin production must be compensated by the total rate of auxin degradation. For translation-invariant steady states this gives immediately $A_c = \beta/\rho$ just like in the one-dimensional model. In addition, A_a^R is determined by the equation

$$0 = 2D(A_c - A_a^R) - 2\alpha N^{AUX1} \frac{A_a^R}{1 + \frac{A_a^R}{A^*} + \frac{A_c}{A^{**}}} + \gamma\sigma^R \frac{A_c}{1 + \frac{A_a^R}{A^*} + \frac{A_c}{A^{**}}}, \quad (16)$$

where $\sigma^R = N_R^{PIN} + N_f^{PIN}$. A^U is determined by the analogous equation in which the index R is replaced by U and $\sigma^U = N_U^{PIN} + N_D^{PIN}$. Thus, in contrast to the one-dimensional case, the concentration of auxin in apoplasts depends not only on model parameters like D but also on PIN polarization. Unpolarized configurations leads to $\sigma^R = \sigma^U = \sigma/2$ and then $A_a^U = A_a^R$, in which case the equations take the same form as in one dimension.

The lowest possible value of A_a^R arises when $\sigma^R = 0$, and the highest value arises when $\sigma^R = \sigma$. These lower and upper bounds are represented in Fig. 10 along with the value of A_c as a function of D . Clearly, auxin concentrations are hardly affected at all by PIN polarization. Furthermore, both qualitatively and quantitatively, the situation is very close to that in the one-dimensional model.

B. Translation-invariant dynamics of PIN in the quasi-equilibrium limit for auxin

In the one-dimensional model, we saw that translation-invariant dynamics of PIN polarization followed from an effective potential when auxin was assumed to be in the quasi-equilibrium state. In two dimensions, there are four dynamical variables which satisfy the conservation law $N_R^{PIN} + N_L^{PIN} + N_U^{PIN} + N_D^{PIN} = \sigma$. Each N_f^{PIN} obeys a first order differential equation; the question now is whether these follow from an effective potential \mathcal{F} :

$$\frac{dN_f^{PIN}}{dt} = -\frac{\partial \mathcal{F}}{\partial N_f^{PIN}} \quad (17)$$

The answer is negative: no effective potential exists because the velocity field has a non-zero curl. Nevertheless, if in the initial conditions the PINs obey the symmetry $N_U^{PIN} = N_D^{PIN}$ (or the symmetry $N_R^{PIN} = N_L^{PIN}$), then this

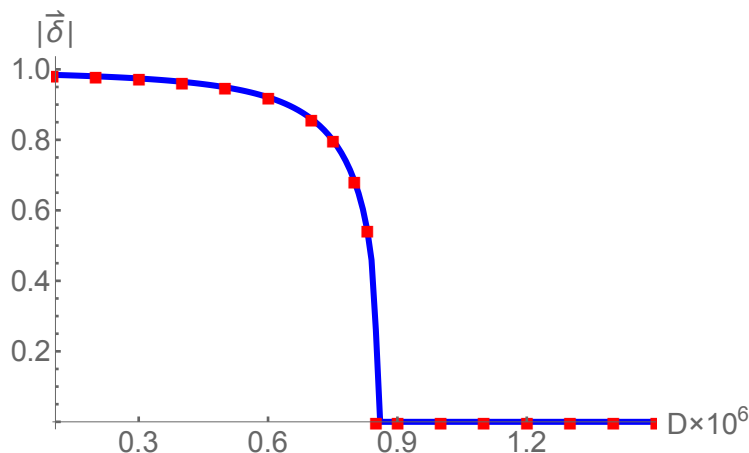


FIG. 11: Norm of the (translation-invariant) polarization vector as a function of the diffusion constant D in $\mu\text{m}^2/\text{s}$ in steady states. Blue circles: analytical result using Mathematica. Red squares: result of simulating the dynamics of the model containing 20×20 cells until a steady state was reached; a fourth-order Runge-Kutta algorithm [32] was used, starting configurations were randomized but had positive local PIN polarizations. $h = 2$, other parameter values are given in Table I.

symmetry is preserved by the dynamics. (Note that the symmetry is associated with reflecting the system of cells along an axis.) Then one sees that the differential equations for the two other PIN numbers are nearly identical to those in the one-dimensional model. For instance, if $N_U^{PIN} = N_D^{PIN}$, the equation for N_R^{PIN} is that of the one-dimensional model if one substitutes σ by σ^R . The difficulty is that σ^R itself follows from solving the differential equations and thus can depend on time. Although one does not have a true effective potential, the important property is that the instantaneous rate of change of N_R^{PIN} can be mapped to its value in the one-dimensional model via the aforementioned substitution. We thus expect to have the same kind of spontaneous symmetry breaking where the unpolarized steady state goes from being stable at low h to being unstable at high h , with an associated appearance of stable polarized steady states.

C. Spontaneous symmetry breaking and phase diagram for translation-invariant steady states

To determine the translation-invariant steady states, one must solve six simultaneous non-linear equations, two of which give A_a^R and A_a^U in terms of the N_f^{PIN} , the other four being associated with PIN recycling. We solve these equations using Mathematica. Qualitatively, one obtains the same behavior as in the one-dimensional model. As displayed in Fig. 11, there is a continuous transition between a polarized state at low D and an unpolarized state at large D . The qualitative justification is as before, *i.e.*, at large D active transport is irrelevant and auxin diffusion leads to unpolarized cells.

To reveal the importance of the parameter h , we show the behavior of the polarization in Fig. 12a. Just as in one dimension, for low values of h there is only one steady state and it is unpolarized. Increasing h , there is spontaneous symmetry breaking at a first threshold where the unpolarized state becomes unstable and a new polarized steady state appears. Cells in that polarized state have a greatest number of PIN transporters on one face and no polarization in the perpendicular direction. Because of this last property, the system effectively behaves as a stack of rows which do not exchange auxin, each row being like the polarized one-dimensional system. Surprisingly, a second spontaneous symmetry breaking transition arises at still larger values of h : two other translation-invariant steady states appear as illustrated in Fig. 12a. However these new states are always linearly unstable and so will not be considered further.

To get a global view of the phase diagram as a function of both D and h , we present via a heat map the complete phase diagram in Fig. 13 where the norm of the polarization vector is given only for the (unique) stable (and translation-invariant) steady state.

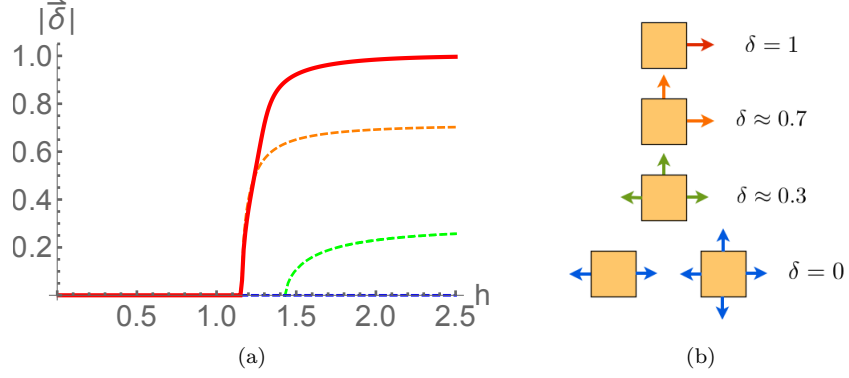


FIG. 12: Left: $|\vec{\delta}|$ in translation-invariant steady states as a function of the Hill exponent h in the low diffusion regime ($D = 10^{-7} \mu\text{m}^2/\text{s}$). Stable steady states are shown in red, the others are linearly unstable. Right: for each type of steady state, we show the corresponding PIN configurations along with the norm of δ in the limit of large h .

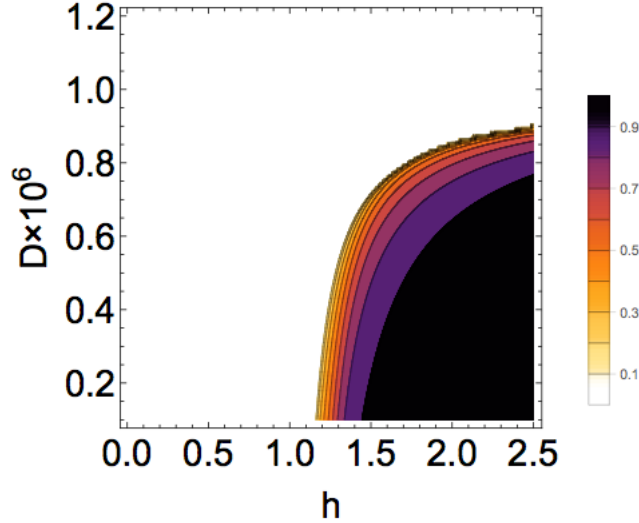


FIG. 13: Heat map of $|\vec{\delta}|$ in translation-invariant steady states as a function of h and D in $\mu\text{m}^2/\text{s}$ rescaled by a factor 10^6 for an easier reading. Other parameter values are given in Table I.

D. Non translation-invariant steady states

Just as in the one-dimensional model, in the limit of large h , each cell can polarize independently, so one has 2^M states if there are M cells. However as h is lowered, far fewer steady states exist because nearby cells tend to align their polarizations. To demonstrate this, we again follow the procedure introduced in the one-dimensional model which allowed us to follow the polarization of one or two defect cells in an otherwise homogenous system. However, in the present two-dimensional case, there are two possibilities: the defect can be polarized in the direction opposite to that of its neighbors as in one dimension, or it can be perpendicular to that direction. Either way, the behavior is similar to what happens in the one-dimensional model, as illustrated in Fig. 15 for the case of perpendicular polarizations.

One can speculate that the larger the domain of cells having similarly oriented polarizations, the greater the stability of the associated steady state and the larger the size of its basin of attraction. Thus for D close to D_c , the dominant steady states (for instance as obtained from relaxing from random initial conditions) should exhibit some local ordering of their polarization patterns. Furthermore, it is plausible that the presence of noise will enhance ordering as it does in one dimension, except that here true long-range order may be possible.

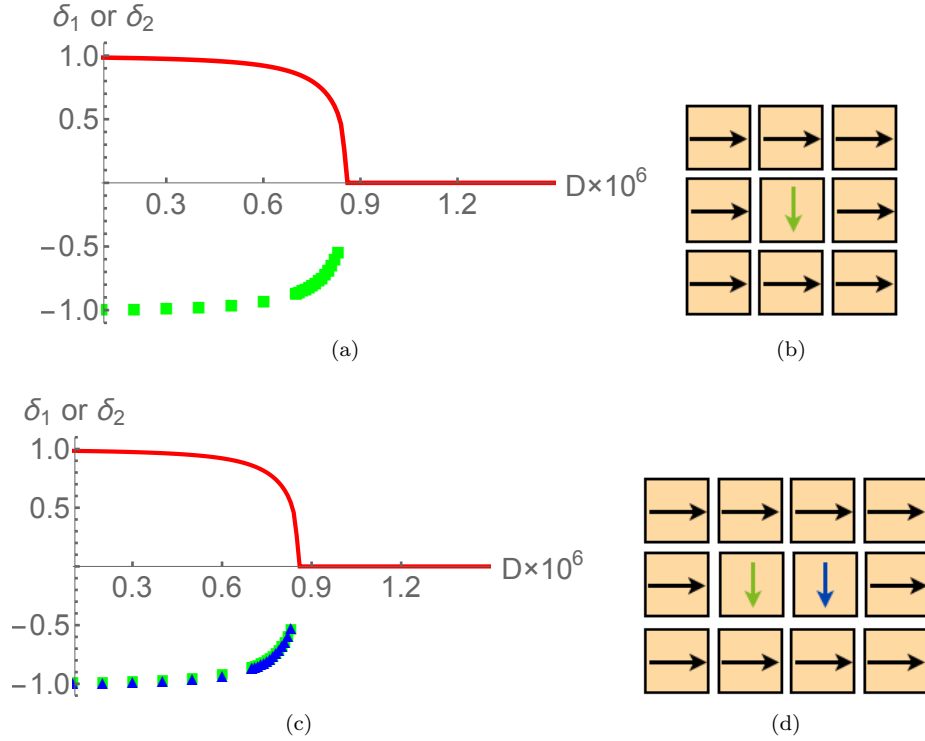


FIG. 14: Diagrams showing the vertical component of the polarization in defect cells as a function of the diffusion constant for respectively one (Fig. 14a) and two defects next to one another (Fig. 14c) in a 10×10 lattice of cells. Also plotted is the polarization intensity in the absence of defects. For $D \geq 8.4 \times 10^{-7}$, the green and blue points are not plotted as they fall on the red curve.

E. Properties of the stochastic model

The method of introducing molecular noise into the dynamical equations is oblivious to the dimensionality of the model. Thus each dynamical equation can be rendered stochastic for the two-dimensional model without any further thought by following the procedure previously described for the one-dimensional case: just consider each underlying flux and go from the average number of molecules transferred in the time step dt to a random number of molecules generated according to a Poisson law with the deterministic average. Ergodicity of the dynamics follows and thus the uniqueness of the “thermodynamic equilibrium state”. We now study that state by simulation on a lattice with periodic boundary conditions.

Initializing the PIN variables to be fully polarized, we thermalize the system and then sample the thermodynamic equilibrium state. To test whether equilibrium is reached, we also used unpolarized initial states and checked whether the initial condition affects the averages obtained from the simulations. Just as in the one-dimensional case at low D , we found that the use of polarized initial conditions led to better thermalization than the use of unpolarized initial conditions.

Once equilibration was observed, we measured the average polarization vector $\langle \vec{\delta} \rangle$, the average $\langle \cdot \rangle$ being taken over the whole lattice at one specific time. We also define θ_P as the angle of that averaged vector, $\tan(\theta_P) = \delta_2/\delta_1$. In the low D regime, the cells stay highly polarized and are oriented close to a common direction along one of the axes of the lattice. This situation illustrated in Fig. 15 where we also show the distribution of θ_P over the time of the simulation. On the contrary, for “high” D , PINs tend to distribute quite evenly amongst the faces of a cell and this leads to a relatively flat histogram for the values of θ_P (Fig. 15). However that histogram is a bit misleading because the polarization vectors $\langle \vec{\delta} \rangle$ have a very small magnitude and in effect each cell is relatively depolarized.

Just as in the one-dimensional case, one may ask whether there is a true transition from a globally polarized state to an unpolarized state when D goes from low to high values. A naive way to do so would be to average $\langle \vec{\delta} \rangle$ over the length of the simulation. However, because the dynamics is ergodic, this average should vanish in the limit of a long run. The same difficulty arises in all systems that undergo spontaneous symmetry breaking. It is necessary to first take the norm of $\langle \vec{\delta} \rangle$, then average over time, and finally check for trends with the size of the lattice. In Fig. 16

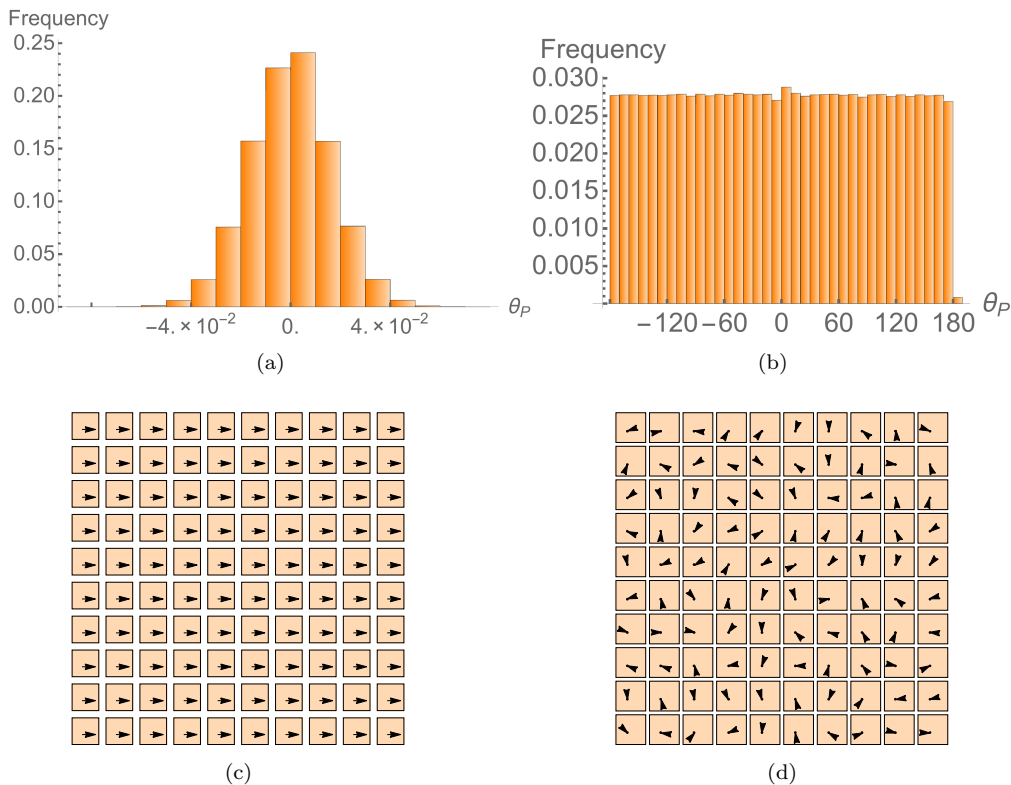


FIG. 15: Top: histograms of the lattice-wide polarization angle, θ_P , in degrees, for the regimes of low (left) and high (right) D , accumulated during a simulation of the model using a 10×10 lattice. Bottom: typical equilibrium configurations in those same two regimes. Left: $D = 10^{-7} \mu\text{m}^2/\text{s}$. Right: $D = 10^{-6} \mu\text{m}^2/\text{s}$.

we show this time average, $|\overline{\langle \vec{\delta} \rangle}|$, as a function of D for lattices of different sizes. For comparison, we also show the corresponding curve in the absence of noise. The behavior displayed is compatible with a true ordering transition as might be expected from the analogy with the behavior of the Ising model. Such a behavior is also in agreement with the noise-induced ordering scenario [38] and related phenomena [33].

V. CONCLUSIONS

Although auxin transport in meristems and the associated molecular actors have been actively studied in the past decade, the questions of how intra-cellular PIN polarisation arises and how globally coherent polarization patterns emerge have not been sufficiently addressed. Our work is based on modeling both auxin transport across cells and PIN recycling within individual cells. The dynamics we use for PIN recycling is modulated by an auxin flux-sensing system. This recycling allows PIN transporters to move within a cell from one face to another. The PINs can accumulate on one face if there is a feedback which allows for a polarization of the cell to maintain itself. Given this framework and estimates for a number of model parameter values, we mapped out a phase diagram giving the system's behavior in terms of specific parameters. The one-dimensional model, describing a row of cells in a meristem, allowed for PIN polarization in the absence of any auxin gradient. Furthermore that toy limit was analytically tractable and correctly described all the features arising in the two-dimensional model. Such a control of the model's properties revealed a particularly essential ingredient: PIN polarization requires a sufficient level of *cooperativity* in the PIN recycling rates. In terms of our mathematical equations, this cooperativity is parametrized by the Hill exponent h appearing in Eq. 5. If there is no cooperativity as in Michaelis-Menten dynamics (corresponding to $h = 1$), the system always goes to the unpolarized state, preventing morphogenesis. But when h rises above a threshold h_c , the homogeneous unpolarized state becomes unstable and polarized PIN patterns spontaneously emerge. Furthermore, by studying the feedback between auxin concentrations and PIN recycling, we showed that nearby cells tend to polarize in the same direction. The other particularly striking result found was that the molecular noise in the PIN recycling dynamics leads to a unique equilibrium state in which the PIN polarization patterns seem to have long range coherence.

Given that these conclusions follow from our hypothesis that PIN recycling is based on flux sensing, experimental

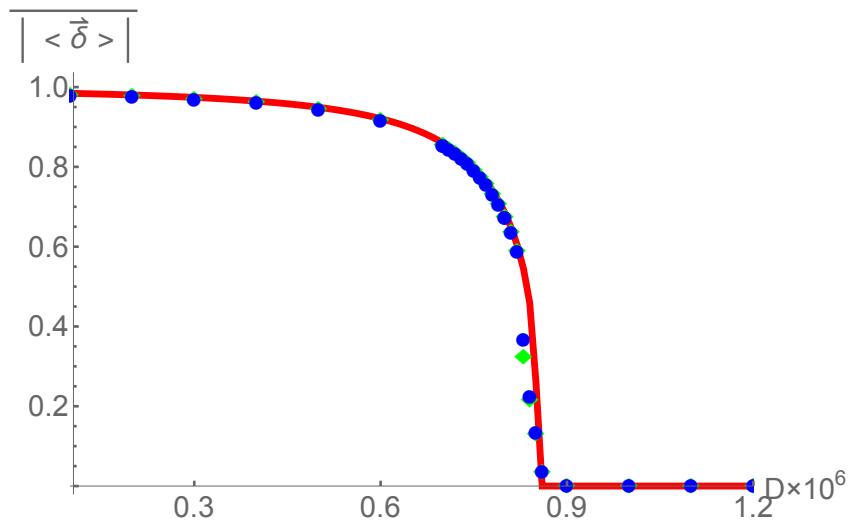


FIG. 16: Time-average of $|\langle \vec{\delta} \rangle|$ as a function of D for a 10×10 lattice size (green diamonds) and for a 5×5 lattice size (blue circles). The deterministic curve is shown as well (red curve). The critical diffusion constant, D_c , is slightly lower when using stochastic dynamics.

investigations should be performed to provide stringent comparisons with our model's predictions. The most direct test of our hypothesis would be to determine whether cells depolarize when the auxin flux carried by PINs is suppressed. In *Arabidopsis*, the polarization of PIN can be observed thanks to fluorescent PIN transporters so what needs to be done is to apply a perturbation affecting auxin flux. One simple way to do so is to inject auxin into an apoplast; the associated increase in auxin concentration will likely inhibit PIN transport into that apoplast. If such an injection cannot be done without mechanically disrupting the cell membranes, a less invasive manipulation could be obtained if it were possible to modify the AUX1 transporters so that they may be locally photo-inhibited. Exposure to a laser beam would then prevent the auxin from leaving a given apoplast, followed by a rapid increase in auxin concentration just as in the simpler experiment previously proposed. Note that in both cases, our model predicts that the PIN recycling dynamics would lead to depolarization of the cell polarized towards the apoplast while the other cell adjacent to the apoplast would hardly be affected.

VI. ACKNOWLEDGEMENTS

We thank Fabrice Besnard and Silvio Franz for critical insights and Barbara Bravi and Bela Mulder for comments. This work was supported by the Marie Curie Training Network NETADIS (FP7, grant 290038).

-
- [1] J. Traas. Phyllotaxis. *Development*, 140:249, 2013.
 - [2] T. Vernoux et al. Auxin at the shoot apical meristem. *Cold Spring Harb Perspect Biol*, 2(a001487), 2010.
 - [3] E. R. Alvarez Buylla et al. *Flower Development*. 2010.
 - [4] B. Scheres. Plant cell identity. the role of position and lineage. *Plant Physiology*, 125, 2001.
 - [5] F.W. Went. Auxin, the plant-growth hormone. ii. *The Botanical Review*, 11(9), 1945.
 - [6] D. Reinhardt et al. Auxin regulates the initiation and radial position of plant lateral organs. *The Plant Cell*, 12(507), 2000.
 - [7] D. Reinhardt et al. Regulation of phyllotaxis by polar auxin transport. *Nature*, 426(255), 2003.
 - [8] K. Palme et al. Pin-pointing the molecular basis of auxin transport. *Current Opinion in Plant Biology*, 2, 1999.
 - [9] G. K. Muday et al. Polar auxin transport: controlling where and how much. *TRENDS in Plant Science*, 6(11), 2001.
 - [10] J. Petràšek et al. Auxin transport routes in plant development. *Development*, 136:2675, 2009.
 - [11] L. Gälweiler et al. Regulation of polar auxin transport by atpin1 in arabidopsis vascular tissue. *Science*, 282, 1998.
 - [12] E. Zazimalová et al. *Auxin and its role in plant development*. Springer, 2014.
 - [13] R. Chen et al. *Polar auxin transport*, volume 17 of *Signaling and communication in plants*. Springer, 2013.
 - [14] P. B. de Reuille et al. computer simulations reveal properties of the cell-cell signaling network at the shoot apex in arabidopsis. *PNAS*, 103(5):1627, 2006.

- [15] R. S. Smith et al. A plausible model of phyllotaxis. *PNAS*, 103(5):1301, 2006.
- [16] H. Jönsson et al. An auxin - driven polarized transport model for phyllotaxis. *PNAS*, 103:1633, 2006.
- [17] J. Kleine Vehn et al. Subcellular trafficking of arabidopsis auxin influx carrier aux1 uses a novel pathway distinct from pin1. *The Plant Cell*, 18:3171, 2006.
- [18] P. Křeček et al. The pin-formed (pin) protein family of auxin transporters. *Genome Biology*, 10(12), 2009.
- [19] I. A. Paponov et al. The pin auxin efflux facilitators: evolutionary and functional perspectives. *TRENDS in Plant Science*, 10(4), 2005.
- [20] E. M. Kramer et al. Auxin transport: a field in flux. *TRENDS in Plant Science*, 11(8), 2006.
- [21] E. M. Kramer. Computer models of auxin transport: a review and commentary. *Journal of Exp. Botany*, 59(1):45, 2007.
- [22] M. Sassi et al. Auxin and self-organization at the shoot apical meristem. *Journal of Exp. Botany*, 64(9):2579, 2013.
- [23] J. Wisniewska et al. Polar pin localization directs auxin flow in plants. *Science*, 312(5775):883, 2006.
- [24] E. Benková et al. Local, efflux-dependent auxin gradients as a common module for plant organ formation. *Cell*, 115, 2003.
- [25] C. Löffke et al. Posttranslational modification and trafficking of pin auxin efflux carriers. *Mechanisms of Development*, 130, 2013.
- [26] H. Tanaka et al. Cell polarity and patterning by pin trafficking through early endosomal compartments in arabidopsis thaliana. *PLoS Genetics*, 9(5), 2013.
- [27] J. Kleine Vehn et al. Recycling, clustering and endocytosis jointly maintain pin auxin carrier polarity at the plasma membrane. *Molecular Systems Biology*, 7, 2011.
- [28] K. van Berkel et al. Polar auxin transport: models and mechanisms. *Development*, 140, 2013.
- [29] K. Wabnik et al. Emergence of tissue polarization from synergy of intracellular and extracellular auxin signaling. *Molecular Systems Biology*, 6(447), 2010.
- [30] E. E. Deinum. *Simple models for complex questions on plant development*. PhD thesis, Wageningen University, 2013.
- [31] K. Ljung et al. Sites and homeostatic control of auxin biosynthesis in arabidopsis during vegetative growth. *The Plant Journal*, 28(4), 2001.
- [32] W. H. Press et al. *Numerical Recipes*. Cambridge University Press, 3rd edition edition, 2007.
- [33] D. Helbing et al. Drift- or fluctuation-induced ordering and self-organization in driven many-particle systems. *Europhys. Lett.*, 60(227), 2002.
- [34] S. Ponce Dawson et al. Lattice boltzmann computation for reaction - diffusion equations. *J. Chem. Phys.*, 98(2), 1993.
- [35] D. T. Gillespie. Exact stochastic simulation of coupled chemical reactions. *The Journal of Physical Chemistry*, 81(25), 1977.
- [36] L. D. Landau et al. *Statistical Physics - Part I and II*, volume 5 of *Course of Theoretical Physics*. Butterworth-Heinemann, 1975.
- [37] K. Huang. *Statistical mechanics*. Wiley, 2nd edition, 1987.
- [38] K. Matsumoto et al. Noise - induced order. *J. Stat. Phys.*, 31(1), 1983.

SUPPLEMENTARY MATERIAL TO: MODELING THE EMERGENCE OF POLARITY PATTERNS IN MERISTEMIC AUXIN TRANSPORT

Appendix A: Linearized auxin dynamics for given PIN configurations

In the Main Text we determined auxin steady states assuming given *translation-invariant* states for PIN. Given such PIN polarizations, we balanced the synthesis and catabolism rates of auxin, concluding that the steady-state concentration of auxin in cells was $A_c = \beta/\rho$. Furthermore, as can be seen in Figure 10 of the Main Text, the concentrations in the horizontal and vertical apoplasts have hardly any dependence on PIN polarization. These features suggest that auxin steady-state concentrations might be only *weakly* dependent on the PIN polarizations, whether these are translation-invariant or not, in which case the linearization of the equations should suffice for an accurate description of auxin dynamics.

In this linearization approach, we take PIN polarizations to be arbitrary but fixed in time, and we introduce the (small) deviations of auxin concentrations compared to a reference state. That reference state can be arbitrary, but for tractability, it will be taken to be translation invariant. Then the study of the linearized equations will provide insights on (i) relaxational dynamics, (ii) the “ferromagnetic” coupling between nearest neighbour cells, and (iii) how the auxin steady state is affected by changes in PIN polarizations.

1. Dynamical equations

For pedagogical reasons, we provide the explicit equations only for the one dimensional case; the equations for the two dimensional model are obtained using the same procedures. In the (translation-invariant) reference state, we take auxin concentration in cells (respectively apoplasts) to be A_c^* (respectively A_a^*). Then we consider (small) deviations

in auxin concentrations, deviations that may vary from cell to cell or apoplast to apoplast:

$$A_c(x, t) = A_c^* + \delta A_c(x, t), \quad A_a(x, x + \Delta, t) = A_a^* + \delta A_a(x, x + \Delta, t)$$

where $\Delta = \Lambda + \lambda$ is the cell to cell distance as defined in the Main Text. The dynamical equations (only for auxin, the PIN transporters being taken as fixed since the recycling time is long) then become:

- for cells:

$$\begin{aligned} \frac{d(A_c^* + \delta A_c(x, t))}{dt} &= \beta - \rho \left[A_c^* + \delta A_c(x, t) \right] + \\ &+ \frac{D}{\Lambda \epsilon} \left[2A_a^* + \delta A_a(x - \Delta, x, t) + \delta A_a(x, x + \Delta, t) - 2A_c^* - 2\delta A_c(x, t) \right] + \\ &+ \frac{\alpha N^{AUX1}}{\Lambda^3} \left[\frac{A_a^* + \delta A_a(x - \Delta, x, t)}{1 + \frac{A_a^* + \delta A_a(x - \Delta, x, t)}{A^*} + \frac{A_c^* + \delta A_c(x, t)}{A^{**}}} \right] + \\ &+ \frac{\alpha N^{AUX1}}{\Lambda^3} \left[\frac{A_a^* + \delta A_a(x, x + \Delta, t)}{1 + \frac{A_a^* + \delta A_a(x, x + \Delta, t)}{A^*} + \frac{A_c^* + \delta A_c(x, t)}{A^{**}}} \right] + \\ &- \frac{\gamma}{\Lambda^3} \left[N_R^{PIN}(x) \frac{A_c^* + \delta A_c(x, t)}{1 + \frac{A_a^* + \delta A_a(x - \Delta, x, t)}{A^*} + \frac{A_c^* + \delta A_c(x, t)}{A^{**}}} + \right. \\ &\left. + N_L^{PIN}(x) \frac{A_c^* + \delta A_c(x, t)}{1 + \frac{A_a^* + \delta A_a(x, x + \Delta, t)}{A^*} + \frac{A_c^* + \delta A_c(x, t)}{A^{**}}} \right], \end{aligned} \tag{A1}$$

where $N_L^{PIN}(x)$ and $N_R^{PIN}(x)$ refer to the PIN transporters lying respectively on the left and right hand-side of the cell C at position x .

- for apoplasts:

$$\begin{aligned} \frac{d(A_a^* + \delta A_a(x, x + \Delta, t))}{dt} &= \frac{D}{\lambda \epsilon} \left[2A_c^* + \delta A_c(x, t) + \delta A_c(x + \Delta, t) - 2A_a^* - 2\delta A_a(x, x + \Delta) \right] + \\ &- \frac{\alpha N^{AUX1}}{\lambda \Lambda^2} \left[\frac{A_a^* + \delta A_a(x, x + \Delta)}{1 + \frac{A_a^* + \delta A_a(x, x + \Delta)}{A^*} + \frac{A_c^* + \delta A_c(x, t)}{A^{**}}} + \frac{A_a^* + \delta A_a(x, x + \Delta)}{1 + \frac{A_a^* + \delta A_a(x, x + \Delta)}{A^*} + \frac{A_c^* + \delta A_c(x + \Delta, t)}{A^{**}}} \right] + \\ &+ \frac{\gamma}{\lambda \Lambda^2} \left[N_R^{PIN}(x) \frac{A_c^* + \delta A_c(x, t)}{1 + \frac{A_a^* + \delta A_a(x, x + \Delta)}{A^*} + \frac{A_c^* + \delta A_c(x, t)}{A^{**}}} + \right. \\ &\left. + N_L^{PIN}(x + \Delta) \frac{A_c^* + \delta A_c(x + \Delta, t)}{1 + \frac{A_a^* + \delta A_a(x, x + \Delta)}{A^*} + \frac{A_c^* + \delta A_c(x + \Delta, t)}{A^{**}}} \right] \end{aligned} \tag{A2}$$

Linearizing for small variations δA_c and δA_a , Eq. A1 becomes:

$$\begin{aligned} \frac{d\delta A_c(x, t)}{dt} &= \beta - \rho \left[A_c^* + \delta A_c(x, t) \right] + \frac{2D}{\Lambda \epsilon} \left[A_a^* - A_c^* \right] + \frac{D}{\Lambda \epsilon} \left[\delta A_a(x - \Delta, x) + \delta A_a(x, x + \Delta) - 2\delta A_c(x, t) \right] + \\ &+ \frac{\alpha N^{AUX1}}{\Lambda^3} \left[\frac{2A_a^*}{1 + \frac{A_a^*}{A^*} + \frac{A_c^*}{A^{**}}} - \frac{\frac{2A_a^*}{A^{**}}}{\left(1 + \frac{A_a^*}{A^*} + \frac{A_c^*}{A^{**}}\right)^2} \delta A_c(x, t) \right] + \\ &+ \frac{\alpha N^{AUX1}}{\Lambda^3} \frac{1 + \frac{A_c^*}{A^{**}}}{\left(1 + \frac{A_a^*}{A^*} + \frac{A_c^*}{A^{**}}\right)^2} \left[\delta A_a(x, x + \Delta) + \delta A_a(x - \Delta, x) \right] + \\ &- \frac{\gamma \sigma}{\Lambda^3} \left[\frac{A_c^*}{1 + \frac{A_a^*}{A^*} + \frac{A_c^*}{A^{**}}} + \frac{1 + \frac{A_a^*}{A^*}}{\left(1 + \frac{A_a^*}{A^*} + \frac{A_c^*}{A^{**}}\right)^2} \delta A_c(x, t) \right] + \\ &+ \frac{\gamma}{\Lambda^3} \frac{\frac{A_c^*}{A^*}}{\left(1 + \frac{A_a^*}{A^*} + \frac{A_c^*}{A^{**}}\right)^2} \left[N_R^{PIN}(x) \delta A_a(x, x + \Delta) + N_L^{PIN}(x) \delta A_a(x - \Delta, x) \right]. \end{aligned} \tag{A3}$$

where σ is the total number of PINs in a cell (σ is the same for all cells). Two kinds of terms can be identified in the previous equation: there are inhomogeneous terms and homogeneous terms (linear in δA_a or δA_c). Gathering together all the terms belonging to each class, we obtain:

$$\frac{d\delta A_c(x, t)}{dt} = f_C + g\delta A_c(x, t) + \left(\Phi + b_{\pi(C^R)} \right) \delta A_a(x, x + \Delta) + \left(\Phi + b_{\pi(C^L)} \right) \delta A_a(x - \Delta, x), \quad (\text{A4})$$

where:

- $f_C = \beta - \rho A_c^* + \frac{2D}{\Lambda\epsilon}(A_a^* - A_c^*) + \frac{2\alpha N^{AUX1}}{\Lambda^3} \frac{A_a^*}{1 + \frac{A_a^*}{A^*} + \frac{A_c^*}{A^{**}}} - \frac{\gamma\sigma}{\Lambda^3} \frac{A_c^*}{1 + \frac{A_a^*}{A^*} + \frac{A_c^*}{A^{**}}}$;
- $g = -\rho - \frac{2D}{\Lambda\epsilon} - \frac{2\alpha N^{AUX1}}{\Lambda^3} \frac{\frac{A_a^*}{A^{**}}}{(1 + \frac{A_a^*}{A^*} + \frac{A_c^*}{A^{**}})^2} - \frac{\gamma\sigma}{\Lambda^3} \frac{1 + \frac{A_a^*}{A^*}}{(1 + \frac{A_a^*}{A^*} + \frac{A_c^*}{A^{**}})^2}$;
- $\Phi = \frac{D}{\Lambda\epsilon} + \frac{\alpha N^{AUX1}}{\Lambda^3} \frac{1 + \frac{A_c^*}{A^{**}}}{(1 + \frac{A_a^*}{A^*} + \frac{A_c^*}{A^{**}})^2}$;
- $b_{\pi(C^s)} = \frac{\gamma N_s^{PIN}}{\Lambda^3} \frac{\frac{A_c^*}{A^{**}}}{(1 + \frac{A_a^*}{A^*} + \frac{A_c^*}{A^{**}})^2}$, where $\pi(C^s)$ shows the dependence of b on the polarisation π of the face s of the cell C .

Note that the inhomogeneous term, f_C , vanishes if the reference state is in fact a steady state.

Proceeding in the same way for apoplasts, Eq. A2 becomes:

$$\lambda \frac{d\delta A_a(x, x + \Delta, t)}{dt} = f_a + \left[p + p_{\pi(C^R)} + p_{\pi(C^L)} \right] \delta A_a(x, x + \Delta) + \left[q_{\pi(C^R)} \delta A_c(x + \Delta, t) + d_{\pi(C^R)} \right] + \left[q_{\pi(C^L)} \delta A_c(x, t) + d_{\pi(C^L)} \right], \quad (\text{A5})$$

where:

- $f_a = 2\frac{D}{\epsilon}(A_c^* - A_a^*) - \frac{2\alpha N^{AUX1}}{\Lambda^2} \frac{A_a^*}{1 + \frac{A_a^*}{A^*} + \frac{A_c^*}{A^{**}}}$;
- $p = -2\frac{D}{\epsilon} - 2\frac{\alpha N^{AUX1}}{\Lambda^2} \frac{1 + \frac{A_c^*}{A^{**}}}{(1 + \frac{A_a^*}{A^*} + \frac{A_c^*}{A^{**}})}$;
- $p_{\pi(C^s)} = -\frac{\gamma}{\Lambda^2} N_s^{PIN} \frac{\frac{A_c^*}{A^{**}}}{(1 + \frac{A_a^*}{A^*} + \frac{A_c^*}{A^{**}})^2}$;
- $q_{\pi(C^s)} = \frac{D}{\epsilon} + \frac{\alpha N^{AUX1}}{\Lambda^2} \frac{\frac{A_c^*}{A^{**}}}{(1 + \frac{A_a^*}{A^*} + \frac{A_c^*}{A^{**}})^2} + \frac{\gamma}{\Lambda^2} N_s^{PIN} \frac{1 + \frac{A_c^*}{A^{**}}}{(1 + \frac{A_a^*}{A^*} + \frac{A_c^*}{A^{**}})^2}$;
- $d_{\pi(C^s)} = \frac{\gamma}{\Lambda^2} N_s^{PIN} \frac{\frac{A_c^*}{A^{**}}}{1 + \frac{A_a^*}{A^*} + \frac{A_c^*}{A^{**}}}$

To simplify these systems of equations, we note that $\lambda \ll \Lambda$ so that the time scale for change of auxin concentrations in apoplasts is far shorter than that in cells. The simple reason is that apoplasts have much smaller volumes so concentrations there change faster when subject to a given flux. We shall thus consider that δA_a is a fast variable in quasi equilibrium with the slower variations of δA_c . In the limit $\lambda/\Lambda \rightarrow 0$, the left-hand side of Eq. A5 vanishes. Thus the right-hand side of that equation also vanishes, leading to an equation that allows us to express $\delta A_a(x, x + \Delta, t)$ in terms of $\delta A_c(x, t)$ and $\delta A_c(x + \Delta, t)$. Substituting this expression into Eq. A4 leads to the following equation for intracellular auxin concentrations:

$$\frac{d\delta A_c(x, t)}{dt} = f_C + g\delta A_c - \sum_{C^s} \left[\Phi + b_{\pi(C^s)} \right] \left[\frac{f_a + d_{\pi(C^s)} + d_{\pi(C'^s')}}{p + p_{\pi(C^s)} + p_{\pi(C'^s')}} + \frac{q_{\pi(C^s)} \delta A_c}{p + p_{\pi(C^s)} + p_{\pi(C'^s')}} + \frac{q_{\pi(C'^s')} \delta A_{C'^s'}}{p + p_{\pi(C^s)} + p_{\pi(C'^s')}} \right] \quad (\text{A6})$$

where we use the notation C^s to refer to the face s of the cell C at x , while C'^s' refers to the associated face s' of cell C' , C^s and C'^s' delimiting the apoplast separating C and C' .

2. Cell-cell couplings are ferromagnetic

It is possible to draw a correspondence between Eq. A6 and the dynamics in standard many body problems. Consider a lattice of continuous variables σ_i , $i = 1, 2, \dots$, whose dynamics is ruled by the Hamiltonian $\mathcal{H}(\{\sigma_i\})$:

$$\mathcal{H}(\{\sigma_i\}) = - \sum_i \sum_j J_{ij} \sigma_i \sigma_j - \sum_i h_i \sigma_i, \quad (\text{A7})$$

where J_{ij} is the coupling between the i -th and the j -th variable while h_i can be thought of a position-dependent external field. In most physical systems, the matrix J couples only nearest neighbours and can have diagonal elements, just as in Eq. A6. The dynamics of the σ variables are given by

$$\frac{d\sigma_i}{dt} = - \frac{\delta \mathcal{H}}{\delta \sigma_i} = \sum_j J_{ij} \sigma_j + h_i \quad (\text{A8})$$

Let us now identify the σ s with the δA_c s. The set of equations obtained from Eq. A6 by running over all N_{cell} cells can be written as an equation for the vector $\delta \vec{A}_c$:

$$\frac{d\vec{A}_c}{dt} = J \delta \vec{A}_c + \vec{h} \quad (\text{A9})$$

where J is a $N_{cell} \times N_{cell}$ coupling matrix while $\delta \vec{A}_c$ and \vec{h} are N_{cell} component vectors.

Using Eq. A6, the effective couplings between two nearest neighbour cells C and C' arises through the faces s and s' sharing the apoplast separating them, leading to:

$$J_{C-C'} = \left[\Phi + b_{\pi(C^s)} \right] \frac{q_{\pi(C's')}}{p + p_{\pi(C^s)} + p_{\pi(C's')}} \quad (\text{A10})$$

Similarly, we find for the self-coupling:

$$J_{C-C} = g - \sum_{C^s} \left[\Phi + b_{\pi(C^s)} \right] \frac{q_{\pi(C^s)}}{p + p_{\pi(C^s)} + p_{\pi(C's')}} \quad (\text{A11})$$

Lastly, the components of the field vector \vec{h} are given by:

$$h_C = f_C - \sum_{C^s} \left[\Phi + b_{\pi(C^s)} \right] \frac{f_a + d_{\pi(C^s)} + d_{\pi(C's')}}{p + p_{\pi(C^s)} + p_{\pi(C's')}} \quad (\text{A12})$$

To understand what the coupling matrix J tells us about the system, we set A_c^* and A_a^* to their values in the steady state when PIN polarization is maximum and positive for all cells. Given the linearization about these values, the derivations of the previous section show that the matrix J depends on the values of PIN polarizations at each site, as it must. We have computed J numerically for a lattice of 20 cells and periodic boundary conditions where all cells had PIN polarization equal to +1 except the cell at position 9 which had PIN polarization equal to -1. Cell number 9 thus corresponds to a defect.

Far away from the defect, one has the same situation as if the defect were absent, and the matrix J is translation invariant. One also has $J_{C-C} < 0$ which is expected given the stability of the steady state: indeed, if one sets $\delta A_c(C, t)$ to a C -independent positive value, the $\delta A_c(C, t)$ should relax to zero with time. Furthermore, we find $J_{C-C'} > 0$ for C and C' nearest neighbours, corresponding to a ferromagnetic interaction. Both of these results are clearly visible in Fig. 17 away from the defect. If auxin dynamics were just of the passive diffusion type, $J_{C-C'}$ would clearly be positive (*cf.* the linear diffusion equation), but we see that neither the active transport processes nor the need to go from cell to cell via apoplasts affect this conclusion. Interestingly, the signs properties of the J matrix elements hold over the whole lattice and in particular around the defect as can be seen in Fig. 17. Note that both the diagonal and off-diagonal elements of J are slightly affected by the defect but not enough for the sign of any element to change.

Not surprisingly, the overall approach can be generalized to the two-dimensional case. The main difference with the one-dimensional case lies in the distinction between the two types of apoplasts, *i.e.*, the up and right hand-side apoplasts, and the fact that one has to deal with the four PIN transporter numbers for each cell (one for each side). Following the same steps, one obtains the expression for the $N_{cell} \times N_{cell}$ matrix J which couples nearest neighbour

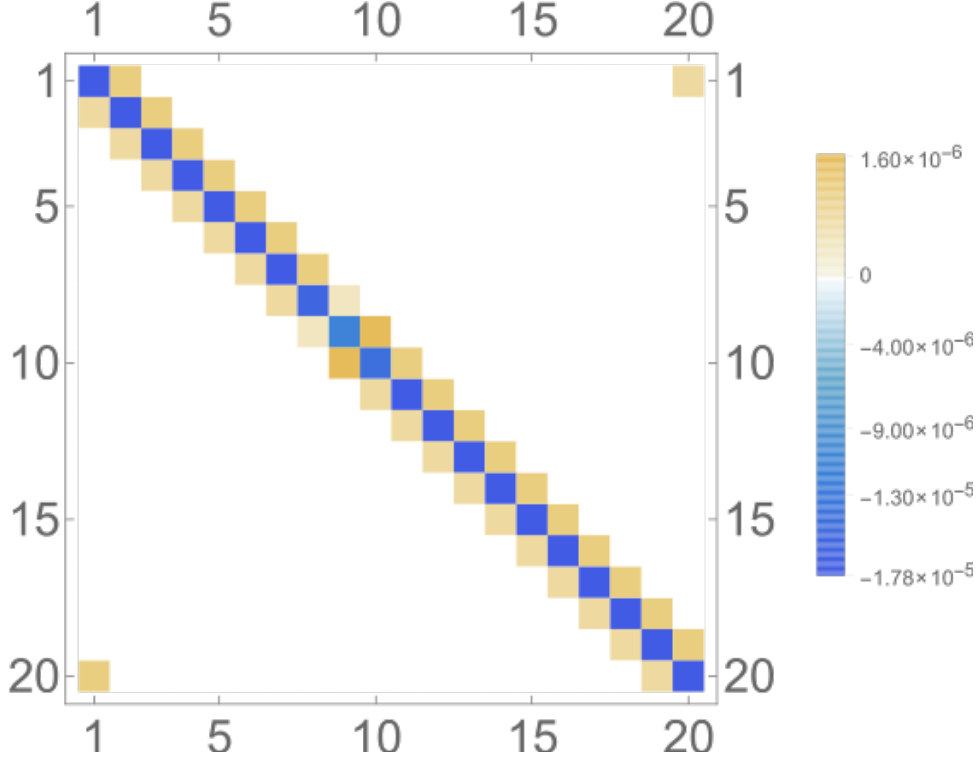


FIG. 17: Heat map of the matrix J obtained for 20 cells in a row that are all maximally polarized in the plus direction but where the cell number 9 is oppositely polarized. $D = 10^{-7} \mu\text{m}^2/\text{s}$, all other parameters are set as in Table I of the Main Text.

cells. The diagonal elements of J are again negative while the off diagonal ones are positive, again indicating effective ferromagnetic couplings between cells.

Lastly, the linearized dynamics (Eqs. A6 or A9) can also be used to probe the steady state auxin concentrations for arbitrary PIN configurations. For illustration, consider again the one-dimensional system of 20 cells that are maximally positively polarized except for cell 9 which has opposite polarization. The steady state in the linearized approximation corresponds to setting the left-hand side of Eq. A9 to zero. The resulting equation gives an estimate of the auxin concentration in each cell, result that is displayed in Fig. 18. By comparing to the exact concentrations (using the full non-linear equations), we see that the linear approximation provides a qualitatively satisfactory description of the changes induced by the defect.

Appendix B: Critical line in the phase diagram

In the Main Text we exploited the effective potential found in the one-dimensional model to obtain the critical diffusion constant D_c . In direct analogy with that calculation, one can obtain the equation for h_c , the critical value of the Hill exponent h . The starting condition is:

$$\left. \frac{\partial^2 \mathcal{F}}{\partial N_R^{PIN^2}} \right|_{N_R^{PIN} = \frac{\sigma}{2}} = 0 \quad (\text{B1})$$

Setting $c = \frac{\gamma}{\lambda^2 \phi^*} \frac{A_c}{1 + \frac{A_a}{A^*} + \frac{A_c}{A^{**}}}$ which depends on D through the dependence on A_a , we obtain:

$$(h-1) \left(\frac{\sigma c}{2} \right)^h = 1 \quad (\text{B2})$$

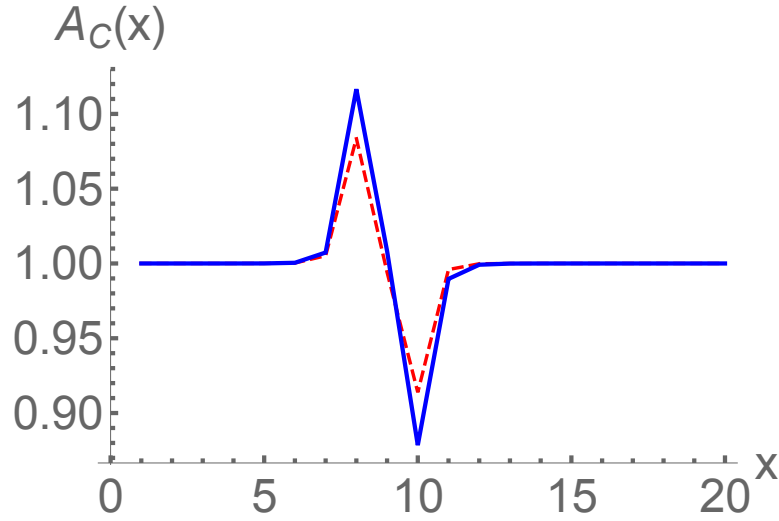


FIG. 18: Auxin concentration in cells as a function of the position along the chain. Blue thick line: prediction of the linearized dynamics. Red dashed line: results from simulation. There is one defect cell at position 9. $D = 10^{-7} \mu\text{m}^2/\text{s}$. All other parameters are set as in the Table in the Main Text. The presence of the defect creates an increase of auxin concentration on its left and a depletion on its right. The linearized approach is qualitatively good but is less precise near the defect.

Applying the logarithm to both the sides, one gets:

$$h = -\frac{\log(h-1)}{\log(\frac{\sigma c}{2})} \quad (\text{B3})$$

This equation provides the critical line in the (D, h) plane (see Main Text, Fig. 6, green dashed line).

Appendix C: Polarisation Angle Susceptibility in the two-dimensional Model

As a follow-up of the last section of the Main Text, it is of interest to consider the variance of the polarisation angle as one approaches the ordering transition at D_c . We thus examine the susceptibility of the angle θ_P , *i.e.*:

$$\chi_{\theta_P} = \overline{\langle \theta_P^2 \rangle - \langle \theta_P \rangle^2} \quad (\text{C1})$$

where the average $\langle \cdot \rangle$ is taken over the lattice and the overline denotes the time average.

In Fig. 19 we show the square root of the susceptibility rescaled by its maximum for different values of D . It stays close to zero (all the polarisation vectors pointing in a similar direction) in the low diffusion regime and then it rises dramatically as one approaches D_c . Clearly once the disordered phase is reached, the variance is maximum and no longer changes with D .

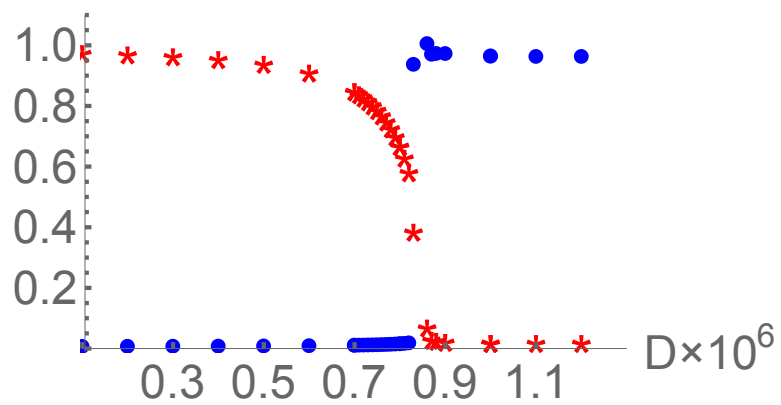


FIG. 19: Rescaled squared root of the normalized angle susceptibility as defined in the text as a function of diffusion constant (blue circles) plotted along with the behaviour of the polarisation (red stars). The steep rise of the susceptibility takes place around the critical value of the diffusion constant as expected.